# New Rectangular Plate Elements Based on Twist-Kirchhoff Theory

F. Brezzi [a,b,*], J.A. Evans [c,†], T.J.R. Hughes [c,‡], and L.D. Marini [d,b,§]

[a] *Istituto Universitario di Studi Superiori, Pavia, Italy*

[b] *Instituto di Matematica Applicata e Tecnologie Informatiche del C.N.R., via Ferrata 3, 27100 Pavia, Italy*

[c] *Institute for Computational Engineering and Sciences, The University of Texas at Austin, 201 East 24th Street, 1 University Station C0200, Austin, TX 78712, USA*

[d] *Dipartimento di Matematica, Università di Pavia, 27100 Pavia, Italy*

## Abstract

We introduce a new framework for the development of thin plate finite elements, the "twist-Kirchhoff theory." A family of rectangular plate elements is derived that takes advantage of the special structure of this new theory. Particular attention is focused on the lowest-order member of the family, an eight degree-of-freedom, four-node element with mid-side rotations whose stiffness matrix is exactly computed with one-point Gaussian quadrature. We prove a convergence theorem for it and various error estimates. These are also generalized to the higher-order elements in the family. Numerical tests corroborate the theoretical results.

**Key words.** plates, finite elements, one-point quadrature, twist-Kirchhoff theory

*Professor of Numerical Analysis

†Graduate Research Assistant

‡Professor of Aerospace Engineering and Engineering Mechanics, Computational and Applied Mathematics Chair III

§Professor of Numerical Analysis

# 1 Introduction

How do we model structures? Well, we use continuum theories, such as elasticity, plasticity, etc., and develop models of solids. However, most structures are designed to carry loads "efficiently," and that usually means they are "thin" and composed of beams, plates, and shells. It seems more finite element analysis of structures has been performed with shell elements than continuum elements (at least that is what one of us was told some time ago by Joop Nagtegaal, corporate fellow of Simulia, the firm marketing Abaqus). The early days of finite element structural analysis were riveted on the development of $C^1$-continuous Poisson-Kirchhoff plate bending elements utilizing interpolations on triangles and quadrilateral element domains. The triumphs of this era were the cubic Clough-Tocher triangle [12], the cubic de Veubeke quadrilateral [15], and the quintic triangular elements of Argyris [1], Cowper [14], and Bell [4]. Unfortunately, these elements were extremely complicated and, due to this, spawned efforts for simpler constructs. (The history of numerical analysis has emphasized time and time again that only the simple survive.) The more general framework of the Reissner-Mindlin shear-deformable theory served as the framework for almost all subsequent developments. On the theoretical side, the work of Brezzi *et al.* [7, 8, 9] firmly established procedures for developing stable and convergent elements within the Reissner-Mindlin framework. On the practical side, Hughes *et al.* [19, 21, 22, 23] and Belytschko *et al.* [5, 6, 17] developed the simplest elements which have enjoyed enormous use in engineering applications. However, the most efficient of these elements, and the ones most used in engineering, are very close to, and unfortunately stray to the wrong side of, the boundary of numerical stability. These are the vaunted "one-point quadrature, four-node quadrilateral elements," the main tools of engineering crash dynamic analysis and sheet metal forming simulations[1]. All of these require "hourglass stabilization," an *ad hoc* and problem-dependent tuning methodology that has been the bane of theorists and, at the very least, an annoyance to practitioners. Despite the thousands of papers on this subject (see [16] for a brief review), a definitive solution, satisfying theorists and practitioners, has never been found. In fact, in recent years, fundamentally new ideas in structural elements have been few and far between. One might even go as far as to say that they have been almost non-existent. We apologize to those readers who may find this statement overly critical, but this is our honest opinion. The search for the holy grail seemed, at least temporarily, to have ended, but perhaps not.

In this paper we explore a new concept for the construction of quadrilateral plate bending elements. In order to prove rigorous convergence theorems and concentrate on the essential ideas, we confine the present development to rectangular plate elements. The lowest-order element is the focus of our attention. We are able to develop a convergent element with only eight degrees of freedom, four vertex transverse displacements and four mid-side normal rotations. Furthermore, in the linear elastic setting, this element is exactly integrated with one-point Gaussian quadrature. The element enjoys full rank and

[1] In explicit dynamic analysis, CPU costs and storage requirements scale with the number of quadrature points, and thus it is of great practical importance to minimize the number of quadrature points.

there are no hourglass modes that need to be stabilized. Here are the key ideas: we work with a plate theory that may be thought of as lying "in between" the classical Reissner-Mindlin and Poisson-Kirchhoff theories. In Reissner-Mindlin theory, bending strains are computed from the derivatives of the rotation field, that is, $\theta_{1,x}$, $\theta_{2,y}$, and $(\theta_{1,y} + \theta_{2,x})/2$. In the present theory, we retain the definitions of the direct components, $\theta_{1,x}$ and $\theta_{2,y}$, but replace $(\theta_{1,y} + \theta_{2,x})/2$ with the twist component of curvature $w_{xy} := w_{,xy}$, where $w$ is the transverse displacement. This amounts to a partial Kirchhoff hypothesis. The variational formulation, referred to as the "twist-Kirchhoff formulation," is otherwise identical to the classical Reissner-Mindlin formulation. However, the twist-Kirchhoff hypothesis restricts applicability of the theory to thin plates. With this form of the bending strains, we are able to utilize very simple interpolations. In particular, on rectangular grids, we can use the lowest-order Raviart-Thomas basis functions for the rotations in which $\theta_1^h$ is piecewise affine in the $x$-direction and constant in the $y$-direction, and $\theta_2^h$ is piecewise affine in the $y$-direction and constant in the $x$-direction. We note that the direct bending strains $\theta_{1,x}^h$ and $\theta_{2,y}^h$ are element-wise constant and thus square-integrable, but the cross derivative terms, $\theta_{1,y}^h$ and $\theta_{2,x}^h$, possess Dirac layers on element boundaries and thus are not square integrable. This is the reason why $\left(\theta_{1,y}^h + \theta_{2,x}^h\right)/2$ is replaced by $w_{xy}^h := w_{,xy}^h$, where $w^h$ is taken to be the standard $C^0$-continuous, piecewise bilinear Lagrange interpolation. Consequently, $w_{xy}^h$ is element-wise constant and square-integrable. We note the complementary nature of the rotation and displacement interpolations, in that $w_{xx}^h := w_{,xx}^h$ and $w_{yy}^h := w_{,yy}^h$ also possess Dirac layers on element boundaries and thus are not square-integrable. As can be seen, the adopted definition of bending strains is the only one possible for such simple interpolations. The final ingredient in the formulation, necessary for its stability, is to use one-point Gaussian quadrature on the transverse shear strains $w_x^h - \theta_1^h$ and $w_y^h - \theta_2^h$, where $w_x^h := w_{,x}^h$ and $w_y^h := w_{,y}^h$. This corresponds exactly to a Lagrange multiplier problem in which the transverse shear force resultants are assumed constant over each element. By virtue of the fact that, in the linear elastic case, the bending energy term is element-wise constant, one-point Gaussian quadrature suffices for the exact evaluation of the entire element stiffness matrix. In summary, for the four-node rectangular plate element $w^h \in \mathbb{Q}_1$, $\theta_1^h, \theta_2^h \in RT_0$, and $\lambda_1^h, \lambda_2^h \in (\mathbb{Q}_0)^2$. The components of the curvature tensor are taken to be $\{\kappa_{11}, \kappa_{22}, \kappa_{12}\} = \left\{\theta_{1,x}^h, \theta_{2,y}^h, w_{xy}^h\right\}$ and thus are constant within each element. By virtue of the fact that the transverse shear force resultants are assumed to be constants on each element, the transverse shear strain components should likewise be viewed as constants. This means that the relevant measures of transverse shear strain are the mean values over elements, or equivalently, the values of shear strain at the $1 \times 1$ Gaussian quadrature point location, which is usually located at the origin of an element isoparametric coordinate system. For a typical rectangular element domain, denoted $R$,

$$\bar{\gamma}_1 = w_x^h(0) - \theta_1^h(0) = \frac{1}{R}\int_R \left(w_x^h - \theta_1^h\right) dR \tag{1}$$

$$\bar{\gamma}_2 = w_y^h(0) - \theta_2^h(0) = \frac{1}{R}\int_R \left(w_y^h - \theta_2^h\right) dR. \tag{2}$$

In this paper, we prove that this element converges to the exact solution of the corre-

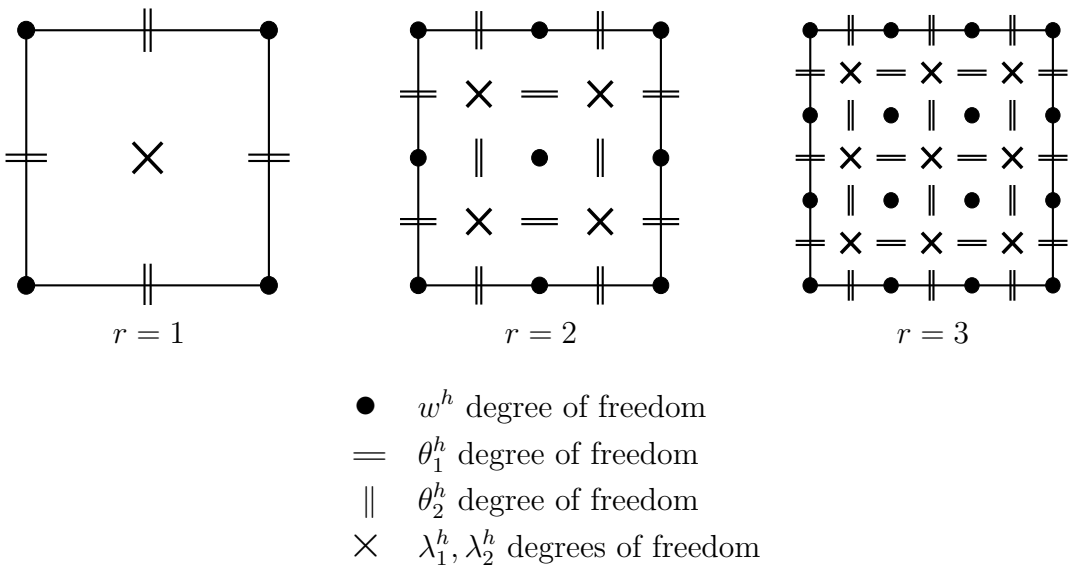


Figure 1: First three members of the new family of finite elements, $w^h \in \mathbb{Q}_r$; $\theta_1^h, \theta_2^h \in RT_{r-1}$; $\lambda_1^h, \lambda_2^h \in (\mathbb{Q}_{r-1})^2$.

sponding continuous theory for the limit problem in which the transverse shear strains are identically zero. The proof is presented for the case of a rectangular plate with two adjacent edges clamped and the other two free. The extension to other boundary conditions, and in particular to the (most mathematically delicate) case of a totally clamped plate, is straightforward. Our proof also applies to the general case, in which the rotations are represented by $H(\mathrm{div})$-conforming Raviart-Thomas vector fields of order $r-1$ (i.e., $RT_{r-1}$, where $r \geq 1$) and the transverse displacement is represented by standard $C^0$-continuous, piecewise bi-Lagrange functions of order $r$ (i.e., $\mathbb{Q}_r$). Stability requires that the transverse shear resultants are interpolated with piecewise discontinuous bi-Lagrange vector fields of one order lower than the transverse displacement, that is, $(\mathbb{Q}_{r-1})^2$. For the formulation of the theory in which the Lagrange multipliers are eliminated, that is the so-called "primal formulation," this implies the use of the $r \times r$-point Gaussian rule on the transverse shear term. The $r \times r$-point Gaussian rule is exact for the bending term, and exact for both bending and transverse terms in the equivalent Lagrange multiplier version. For this latter reason the $r \times r$-point rule should *not* be thought of as a "reduced" quadrature rule. Rather, it is the exact rule for the equivalent Lagrange multiplier version of the formulation and this is the one for which we have stability and convergence proofs. The first three members of the family of elements are schematically illustrated in Figure 1. Numerical tests are performed for the lowest-order member (i.e., $r = 1$) and for $r = 2$. In all cases, the theoretical convergence rates are confirmed.

The remainder of the paper is organized as follows: In Sections 2 and 3 we present the primal and Lagrange multiplier forms of the twist-Kirchhoff theory for a simple model problem. In Section 4 we describe the Lagrange multiplier discretized problem. Error estimates for the discrete approximation of the "limit problem" (i.e., Kirchhoff limit) are

presented in Section 5. Some of the proofs are technical and, so as not to encumber the presentation of the main ideas, details are relegated to Appendices A and B. Preliminary one-dimensional results are derived in Appendix A and the proof of the main theorem appears in Appendix B. Numerical tests are described in Section 6 and conclusions and future directions are summarized in Section 7.

# 2 Theory: Primal Form

Throughout the paper, for $s$ an integer and $\mathcal{O}$ a bounded open set in $\mathbb{R}^n$ ($n = 1$ or 2) we will denote by $\|\cdot\|_{s,\mathcal{O}}$ the usual Sobolev norm in $H^s(\mathcal{O})$ (or copies of it). On the other hand, for $s_1$, $s_2$ nonnegative integers and $\mathcal{O}$ a bounded open set in $\mathbb{R}^2$, $\|\cdot\|_{[s_1,s_2],\mathcal{O}}$ will denote the norm in $H^{s_1,s_2}(\mathcal{O})$, that is

$$\|\phi\|^2_{[s_1,s_2],\mathcal{O}} := \sum_{\alpha\le s_1,\,\beta\le s_2} |\phi|^2_{[\alpha,\beta],\mathcal{O}} \qquad |\phi|^2_{[\alpha,\beta],\mathcal{O}} := \int_{\mathcal{O}} \Big(\frac{\partial^{\alpha+\beta}\phi}{\partial^\alpha x\,\partial^\beta y}\Big)^2\,dx\,dy \tag{3}$$

where obviously $\alpha$ and $\beta$ are assumed to be nonnegative integers.

Let $\Omega$ be the rectangle $]0, L_1[\times]0, L_2[$. Without loss of generality we can assume that $L_1 \le L_2$. We introduce the spaces

$$H_x := \{v \in L^2(\Omega) \text{ such that } v_x \in L^2(\Omega)\} \equiv H^{1,0}(\Omega) \tag{4}$$

$$H_y := \{v \in L^2(\Omega) \text{ such that } v_y \in L^2(\Omega)\} \equiv H^{0,1}(\Omega) \tag{5}$$

$$H_{xy} := \{v \in H^1(\Omega) \text{ such that } v_{xy} \in L^2(\Omega)\} \equiv H^{1,1}(\Omega) \tag{6}$$

$$\boldsymbol{\Theta} := \{\boldsymbol{\theta} = (\theta_1, \theta_2) \in (L^2(\Omega))^2 \text{ such that } \theta_1 \in H_x \text{ and } \theta_2 \in H_y\} \tag{7}$$

$$\boldsymbol{\Theta}_0 := \{\boldsymbol{\theta} \in \boldsymbol{\Theta} \text{ such that } \theta_1 = 0 \text{ for } x = 0, \text{ and } \theta_2 = 0 \text{ for } y = 0\} \tag{8}$$

$$W := \{v \in H_{xy} \text{ such that } v = 0 \text{ on } \partial\Omega\} \equiv H^1_0(\Omega) \cap H_{xy} \tag{9}$$

and, for each subset $\mathcal{O}$ of $\Omega$ the norms and semi-norms

$$|\boldsymbol{\theta}|^2_{(H_x,H_y),\mathcal{O}} := \|\theta_{1,x}\|^2_{0,\mathcal{O}} + \|\theta_{2,y}\|^2_{0,\mathcal{O}}, \qquad \|\boldsymbol{\theta}\|^2_{(H_x,H_y),\mathcal{O}} := \|\boldsymbol{\theta}\|^2_{0,\mathcal{O}} + |\boldsymbol{\theta}|^2_{(H_x,H_y),\mathcal{O}} \qquad \forall \boldsymbol{\theta} \in \boldsymbol{\Theta} \tag{10}$$

$$|v|^2_{H_{xy},\mathcal{O}} := \|v_{xy}\|^2_{0,\mathcal{O}}, \qquad \|v\|^2_{H_{xy},\mathcal{O}} := \|v\|^2_{0,\mathcal{O}} + \|\nabla v\|^2_{0,\mathcal{O}} + 2|v|^2_{H_{xy},\mathcal{O}} \qquad \forall v \in H_{xy} \tag{11}$$

where, here and in all the sequel, we use the notation $\|\cdot\|_{0,\mathcal{O}}$ and $(\cdot\,,\cdot)_{0,\mathcal{O}}$ for the norm and the scalar product (respectively) in $L^2(\mathcal{O})$ or copies of it. In general, the subscript $\mathcal{O}$ will be omitted whenever $\mathcal{O} \equiv \Omega$.

The spaces $\boldsymbol{\Theta}_0$ and $W$ are the spaces of admissible *rotations* and *transverse displacements* respectively.

**Lemma 2.1.** *We have*

$$\|\boldsymbol{\theta}\|^2_0 \le L_1^2\|\theta_{1,x}\|^2_0 + L_2^2\|\theta_{2,y}\|^2_0 \le L_2^2|\boldsymbol{\theta}|^2_{(H_x,H_y)} \qquad \forall \boldsymbol{\theta} \in \boldsymbol{\Theta}_0. \tag{12}$$

*Proof.* The result is well known, being essentially the Poincaré inequality. Start with

$$\theta_1(x,y) = \int_0^x \frac{\partial \theta_1}{\partial x}(t,y)dt \qquad (\text{since } \theta_1(0,y) = 0 \ \forall y), \tag{13}$$

take the square, and apply Cauchy-Schwarz:

$$\theta_1^2(x,y) = \Big( \int_0^x \frac{\partial \theta_1}{\partial x}(t,y)dt \Big)^2 \leq \Big( \int_0^x 1^2 dt \Big) \Big( \int_0^x \big(\frac{\partial \theta_1}{\partial x}(t,y)\big)^2 dt \Big) = \\ x \int_0^x \big(\frac{\partial \theta_1}{\partial x}(t,y)\big)^2 dt \leq L_1 \int_0^{L_1} \big(\frac{\partial \theta_1}{\partial x}(t,y)\big)^2 dt. \tag{14}$$

Integrating the above equation over $\Omega$ we have then

$$\int_\Omega \theta_1^2(x,y)\, dx\, dy \leq L_1^2 \int_\Omega \big(\frac{\partial \theta_1}{\partial x}(x,y)\big)^2 \, dx\, dy. \tag{15}$$

By the same argument we prove that

$$\int_\Omega \theta_2^2(x,y)\, dx\, dy \leq L_2^2 \int_\Omega \big(\frac{\partial \theta_2}{\partial y}(x,y)\big)^2 \, dx\, dy \tag{16}$$

and the result follows. □

**Lemma 2.2.** *We have*

$$\|v\|_0^2 + L_1^2 \|v_x\|_0^2 + L_2^2 \|v_y\|_0^2 \leq 3\ L_1^2 L_2^2\ |v|_{H_{xy}}^2 \quad \forall v \in W. \tag{17}$$

*Proof.* This result too is well known, being strongly related to Poincaré inequality. Arguing as in (13)-(15) we prove that

$$\|v\|_0^2 \leq L_1^2\, \|v_x\|_0^2, \tag{18}$$

while arguing as in (16) we get

$$\|v\|_0^2 \leq L_2^2\, \|v_y\|_0^2. \tag{19}$$

On the other hand, still arguing as in (13)-(15) (and taking into account that if $v = 0$ on $\partial\Omega$ then $v_y = 0$ for $x = 0$) we prove that

$$\|v_y\|_0^2 \leq L_1^2\, |v|_{H_{xy}}^2, \tag{20}$$

and similarly

$$\|v_x\|_0^2 \leq L_2^2\ |v|_{H_{xy}}^2. \tag{21}$$

The result then easily follows. □

We define the space

$$\mathcal{U} := \boldsymbol{\Theta}_0 \times W \tag{22}$$

and equip it with the norm

$$\|V\|_{\mathcal{U}}^2 := \|\boldsymbol{\eta}\|_{(H_x,H_y)}^2 + \|v\|_{H_{xy}}^2 \qquad \text{for } V = (\boldsymbol{\eta}, v), \tag{23}$$

and for every $t > 0$ we define the bilinear form $\mathcal{A}_t$ on $\mathcal{U} \times \mathcal{U}$ as

$$\mathcal{A}_t(U, V) := (\theta_{1,x}, \eta_{1,x})_0 + (\theta_{2,y}, \eta_{2,y})_0 + 2(w_{xy}, v_{xy})_0 + t^{-2}(\nabla w - \boldsymbol{\theta}, \nabla v - \boldsymbol{\eta})_0 \tag{24}$$

for $U = (\boldsymbol{\theta}, w)$ and $V = (\boldsymbol{\eta}, v)$. The *bending part* of the bilinear form $\mathcal{A}_t$ will be denoted by $\mathcal{A}_b$, i.e.,

$$\mathcal{A}_b(U, V) := (\theta_{1,x}, \eta_{1,x})_0 + (\theta_{2,y}, \eta_{2,y})_0 + 2(w_{xy}, v_{xy})_0. \tag{25}$$

The remaining part of the bilinear form $\mathcal{A}_t$ contains the *transverse shear strain* contributions.

We now fix a function (load) $g \in L^2(\Omega)$ and define

$$(G, V)_0 := (g, v)_0 \qquad \text{for } V = (\boldsymbol{\eta}, v). \tag{26}$$

Finally, for every $t > 0$ we define on $\mathcal{U}$ the functional

$$\begin{aligned} J_t^{TK}(V) &:= \frac{1}{2}\mathcal{A}_t(V, V) - (G, V)_0 \\ &\equiv \frac{1}{2}|\boldsymbol{\eta}|_{(H_x,H_y)}^2 + |v|_{H_{xy}}^2 + \frac{t^{-2}}{2}\|\nabla v - \boldsymbol{\eta}\|_0^2 - (g, v)_0. \end{aligned} \tag{27}$$

This is the functional for the primal form of the *twist-Kirchhoff theory* for a simple model plate. The general isotropic plate problem is addressed in Remark 2.2.

**Remark 2.1.** *We are interested in the case "t small". Hence, even when it is not explicitly said, we will not consider the case of t being very big. Let us say that we assume $t \ll L_1$.*

**Proposition 2.1.** *The bilinear form $\mathcal{A}_b$ is continuous and elliptic on $\mathcal{U} \times \mathcal{U}$. More precisely we have*

$$\mathcal{A}_b(U, V) \leq \|U\|_{\mathcal{U}} \|V\|_{\mathcal{U}} \qquad \forall\, U,\, V \in \mathcal{U} = \boldsymbol{\Theta}_0 \times W, \tag{28}$$

*and there exists a constant $\alpha > 0$ such that*

$$\mathcal{A}_b(V, V) \geq \alpha \|V\|_{\mathcal{U}}^2 \qquad \forall\, V \in \mathcal{U} = \boldsymbol{\Theta}_0 \times W. \tag{29}$$

*Proof.* The proof of (28) is an immediate consequence of the definitions (10), (11), and (25). The proof of (29) also follows immediately, from the same definitions and from Lemmata 2.1 and 2.2. □

**Proposition 2.2.** *The bilinear form $\mathcal{A}_t$ is continuous and elliptic on $\mathcal{U}\times\mathcal{U}$. In particular we obviously have from* (29) *that*

$$\mathcal{A}_t(V,V) \geq \mathcal{A}_b(V,V) \geq \alpha\|V\|^2_{\mathcal{U}} \qquad \forall\, V \in \mathcal{U} = \mathbf{\Theta}_0 \times W \tag{30}$$

*and we for every $t > 0$ in there exist a constants $C_t$ such that*

$$\mathcal{A}_t(U,V) \leq C_t\, \|U\|_{\mathcal{U}}\, \|V\|_{\mathcal{U}} \qquad \forall\, U,\, V \in \mathcal{U} = \mathbf{\Theta}_0 \times W, \tag{31}$$

*Proof.* We already noted that (30) is obvious. In its turn, for every $t > 0$ (31) follows immediately from (28). □

**Proposition 2.3.** *Let $U_t^{TK} = (\boldsymbol{\theta}_t^{TK}, w_t^{TK}) \in \mathcal{U}$ be the unique solution of*

$$\mathcal{A}_t(U_t^{TK}, V) = (G,V)_0 \qquad \forall\, V \in \mathcal{U}. \tag{32}$$

*Then, there exists a constant $C > 0$, independent of $t$, such that*

$$\|U_t^{TK}\|^2_{\mathcal{U}} \leq C \qquad \forall\, t > 0, \tag{33}$$

$$\|\boldsymbol{\theta}_t^{TK} - \nabla w_t^{TK}\|_0^2 \leq C\, t^2 \qquad \forall\, t > 0. \tag{34}$$

*Proof.* We first observe that $J_t^{TK}(U_t^{TK}) \leq J_t^{TK}(0) \equiv 0$ (since $U_t^{TK}$ is the minimizer). Hence:

$$\frac{1}{2}|\boldsymbol{\theta}_t^{TK}|^2_{(H_x,H_y)} + |w_t^{TK}|^2_{H_{xy}} + \frac{t^{-2}}{2}\|\nabla w_t^{TK} - \boldsymbol{\theta}_t^{TK}\|_0^2 \leq (g, w_t^{TK})_0 \leq \|g\|_0\, \|w_t^{TK}\|_0.$$

The proof then easily follows from the arithmetic-geometric mean inequality and Lemmata 2.1 and 2.2. □

**Remark 2.2.** *For a general isotropic twist-Kirchhoff plate, the bending part of the bilinear form $\mathcal{A}_t$ takes the form*

$$\mathcal{A}_b(U,V) := \sum_{1\leq\alpha,\beta,\gamma,\delta\leq 2} \left(A_{\alpha\beta\gamma\delta}\kappa_{\gamma\delta}, \bar{\kappa}_{\alpha\beta}\right)_0 \tag{35}$$

*where*

$$A_{\alpha\beta\gamma\delta} = \frac{1}{12}\left[(\delta_{\alpha\gamma}\delta_{\beta\delta} + \delta_{\alpha\delta}\delta_{\beta\gamma}) + \frac{\bar{\lambda}}{\mu}\delta_{\alpha\beta}\delta_{\gamma\delta}\right] \tag{36}$$

*and the curvature tensor components are taken to be*

$$\kappa_{11} = \theta_{1,x}, \kappa_{22} = \theta_{2,y}, \kappa_{12} = \kappa_{21} = w_{xy}, \tag{37}$$

$$\bar{\kappa}_{11} = \eta_{1,x}, \bar{\kappa}_{22} = \eta_{2,y}, \bar{\kappa}_{12} = \bar{\kappa}_{21} = v_{xy}. \tag{38}$$

*In Equation* (36)*, $\delta_{\alpha\beta}$ is the Kroenecker delta and*

$$\bar{\lambda} = \frac{\nu E}{1-\nu^2} \tag{39}$$

$$\mu = \frac{E}{2\,(1+\nu)} \tag{40}$$

*with $E$ and $\nu$ being the Young's modulus and Poisson's ratio, respectively. In addition, for an isotropic plate, one takes the forcing function $g$ to be*

$$g = \frac{1}{\mu t^3} q \tag{41}$$

*where $q$ is the loading per unit area normal to the plate. The theoretical results for the simple model plate presented in this paper extend in a straight-forward manner to the general isotropic case.*

# 3 Theory: Lagrange Multiplier Form

We now introduce the formulation with multipliers. For this we need to define the spaces

$$\mathcal{H} := \left(L^2(\Omega)\right)^2 \tag{42}$$

and

$$Q := \{\boldsymbol{\mu} \in \mathcal{H} \text{ such that } \exists V = (\boldsymbol{\eta}, v) \in \mathcal{U}, \quad \text{with } \boldsymbol{\mu} = \boldsymbol{\eta} - \nabla v\} \tag{43}$$

with the norm

$$\|\boldsymbol{\mu}\|_Q := \inf_{\boldsymbol{\eta} - \nabla v = \boldsymbol{\mu}} \|(\boldsymbol{\eta}, v)\|_{\mathcal{U}} \tag{44}$$

where, obviously, the infimum is taken over the pairs $(\boldsymbol{\eta}, v) \in \mathcal{U}$. We then define the space of multipliers $\mathcal{M}$ as

$$\mathcal{M} := Q' \tag{45}$$

(that is, the dual space of $Q$). It is evident that $Q \subseteq \mathcal{H}$ with continuous dense embedding so that $\mathcal{H}$ (that we identify as usual with its own dual space) can be identified with a dense subspace of $\mathcal{M} = Q'$.

It will be convenient to introduce the operator $B : \mathcal{U} \to Q$ defined as

$$B(V) = \nabla v - \boldsymbol{\eta} \qquad \text{for } V = (\boldsymbol{\eta}, v). \tag{46}$$

Note that definition (43) could be rewritten as $Q :=$ range of $B$, and we have immediately from (44) that $B$, from $\mathcal{U}$ into $Q$ is continuous, surjective, and with a bounded inverse. Hence we have the classical *inf-sup* condition: there exists $\beta > 0$ such that

$$\inf_{\boldsymbol{\mu} \in \mathcal{M}} \sup_{V \in \mathcal{U}} \frac{{}_{\mathcal{M}}< \boldsymbol{\mu}, B(V) >_Q}{\|\boldsymbol{\mu}\|_{\mathcal{M}} \, \|V\|_{\mathcal{U}}} \geq \beta. \tag{47}$$

With the above terminology defined, we are interested in the following saddle-point problem:

$$\begin{cases} \text{Find } U \equiv (\boldsymbol{\theta}, w) \in \mathcal{U} \text{ and } \boldsymbol{\lambda} \in \mathcal{H} \text{ such that} \\ \mathcal{A}_b(U, V) + {}_{\mathcal{M}}< \boldsymbol{\lambda}, B(V) >_Q = (G, V)_0 \quad \forall V \in \mathcal{U} \\ {}_{\mathcal{M}}< \boldsymbol{\mu}, B(U) >_Q - t^2 (\boldsymbol{\lambda}, \boldsymbol{\mu})_0 = 0 \quad \forall \boldsymbol{\mu} \in \mathcal{H}. \end{cases} \tag{48}$$

For $t > 0$ existence and uniqueness of the solution of (48) in $\mathcal{U} \times (L^2(\Omega))^2$ follow from (29).

# 4 The Discretized Problem

Let us consider, for simplicity, a sequence of decompositions $\mathcal{T}_h$ of our domain $\Omega$ into rectangles $R = R_{i,j}$ by means of the points

$$0 \equiv x_0 < x_1 < ... < x_I \equiv L_1 \qquad 0 \equiv y_0 < y_1 < ... < y_J \equiv L_2. \tag{49}$$

We define, as usual, the mesh sizes

$$h_x := \max_{1\le i\le I}(x_i - x_{i-1}) \quad h_y := \max_{1\le j\le J}(y_j - y_{j-1}) \quad h := \max\{h_x, h_y\}. \tag{50}$$

We introduce now the piecewise polynomial spaces

$$\mathcal{L}^s_p := \{v \in H^s(0, L_1) : v_{|(x_{i-1},x_i)} \in \mathbb{P}_p \quad \forall i = 1, ..., I\} \tag{51}$$

$$\mathcal{L}^t_q := \{v \in H^t(0, L_2) : v_{|(y_{j-1},y_j)} \in \mathbb{P}_q \quad \forall j = 1, ..., J\} \tag{52}$$

and the spaces $\mathcal{L}^{s,t}_{[p,q]}$

$$\mathcal{L}^{s,t}_{[p,q]} := \{v \in L^2(\Omega) \; s.t. \; v(\cdot, y^*) \in \mathcal{L}^s_p \; \forall y^* \in ]0, L_2[ \text{ and } v(x^*, \cdot) \in \mathcal{L}^t_q \; \forall x^* \in ]0, L_1[\}. \tag{53}$$

We point out explicitly that for $s = 1$ the elements of $\mathcal{L}^1_r$ belong to $C^0([a, b])$ while for $s = 2$ the elements of $\mathcal{L}^2_r$ belong to $C^1([a, b])$. Obviously for $s = 0$ the elements of $\mathcal{L}^0_r$ might be discontinuous from one element to another.

We now define, for every integer $r \ge 1$ the discrete rotation space as

$$\boldsymbol{\Theta}^h := \boldsymbol{\Theta}_0 \cap \left(\mathcal{L}^{1,0}_{[r,r-1]} \times \mathcal{L}^{0,1}_{[r-1,r]}\right), \tag{54}$$

the discrete transverse displacement space as

$$W^h := W \cap \mathcal{L}^{1,1}_{[r,r]} \tag{55}$$

and the discrete multiplier space as

$$\mathcal{M}^h := \mathcal{L}^{0,0}_{[r-1,r-1]}. \tag{56}$$

Note that, in other terms, $\boldsymbol{\Theta}^h$ is the Raviart-Thomas space of order $r - 1$, $W^h$ is the space of piecewise continuous bi-Lagrange polynomials of order $r$, and $\mathcal{M}^h$ is the space of piecewise discontinuous bi-Lagrange polynomials of order $r - 1$.

**Remark 4.1.** *For $r = 1$, $\theta^h_1$ takes the general form $\theta^h_1 = a_1 + b_1 x$ (with $a_1$ and $b_1$ constants) in each element and is continuous across the vertical interelement boundaries, while $\theta^h_2$ take the general form $\theta^h_2 = a_2 + c_2 y$ (with $a_2$ and $c_2$ constants) in each element and is continuous across the horizontal interelement boundaries. Further, the transverse displacement $w^h$ takes the general form $w^h = a_3 + b_3 x + c_3 y + d_3 xy$ in each element (with $a_3, b_3, c_r$ and $d_3$ constants) and is continuous all over the domain, and the multiplier $\boldsymbol{\lambda}^h$ is a constant vector element-wise. It is easy to see that on each element $R$, all of the integrals necessary to evaluate $\mathcal{A}_t$ can be computed* **exactly** *using a one point Gauss integration formula.*

We can now set $\mathcal{U}^h := \boldsymbol{\Theta}^h \times W^h$ and consider the discrete problem:

$$\begin{cases} \text{Find } U^h \equiv (\boldsymbol{\theta}^h, w^h) \in \mathcal{U}^h, \text{ and } \boldsymbol{\lambda}^h \in \mathcal{M}^h \text{ such that} \\ \mathcal{A}_b(U^h, V) + (\boldsymbol{\lambda}^h, B(V))_0 = (G, V)_0 \quad \forall V \in \mathcal{U}^h \\ (\boldsymbol{\mu}, B(U^h))_0 - t^2(\boldsymbol{\lambda}^h, \boldsymbol{\mu})_0 = 0 \quad \forall \boldsymbol{\mu} \in \mathcal{M}^h. \end{cases} \tag{57}$$

Existence and uniqueness of the solution of the discrete problem follow exactly as for the continuous one.

As we are interested in studying the convergence of $U^h$ to $U$ for (very) small $t$, it seems reasonable to consider, as a first indication, the behavior of the *limit problems* (for $t \to 0$):

$$\begin{cases} \text{Find } U \equiv (\boldsymbol{\theta}, w) \in \mathcal{U} \text{ and } \boldsymbol{\lambda} \in \mathcal{M} \text{ such that} \\ \mathcal{A}_b(U, V) + {}_{\mathcal{M}}{<} \boldsymbol{\lambda}, B(V) {>}_Q = (G, V)_0 \quad \forall V \in \mathcal{U} \\ {}_{\mathcal{M}}{<} \boldsymbol{\mu}, B(U) {>}_Q = 0 \quad \forall \boldsymbol{\mu} \in \mathcal{M} \end{cases} \tag{58}$$

and

$$\begin{cases} \text{Find } U^h \equiv (\boldsymbol{\theta}^h, w^h) \in \mathcal{U}^h, \text{ and } \boldsymbol{\lambda}^h \in \mathcal{M}^h \text{ such that} \\ \mathcal{A}_b(U^h, V) + (\boldsymbol{\lambda}^h, B(V))_0 = (G, V)_0 \quad \forall V \in \mathcal{U}^h \\ (\boldsymbol{\mu}, B(U^h))_0 = 0 \quad \forall \boldsymbol{\mu} \in \mathcal{M}^h. \end{cases} \tag{59}$$

Existence and uniqueness of the solution of (58) follow from (30) and (47). On the other hand, for the existence and uniqueness of the solution of (59) we also need the following results.

**Lemma 4.1.** *Let the spaces $\boldsymbol{\Theta}^h$, and $\mathcal{M}^h$ be defined as in* (54) *and* (56)*, and let $\boldsymbol{\mu} \in \mathcal{M}^h$ be such that*

$$(\boldsymbol{\mu}, \boldsymbol{\eta})_0 = 0 \quad \forall \boldsymbol{\eta} \in \boldsymbol{\Theta}^h. \tag{60}$$

*Then $\boldsymbol{\mu} = 0$.*

*Proof.* We sketch the proof for the lowest order case $r = 1$. In the other cases the proof is quite similar and equally easy. Let $\boldsymbol{\eta} = (\eta_1, 0)$, with $\eta_1 = 1$ at the right boundary of the last element to the right in the lowest row, and zero on all other elements. It follows that $\mu_1 = 0$ in the lowest right element. By taking now $\eta_1 = 1$ at the left boundary of the lowest right element and zero on all other elements (except, of course, on the element before the last, always in the lowest row), we deduce $\mu_1 = 0$ in the element before the last, in the lowest row. Continuing this iterative procedure, we find $\mu_1 = 0$ for the entire lowest row of elements, and repeating this procedure for all the rows, we find that $\mu_1$ is identically zero in $\Omega$. An analogous procedure shows that $\mu_2$ is identically zero as well. □

**Proposition 4.1.** *Let the spaces $\mathcal{U}^h := \boldsymbol{\Theta}^h \times W^h$ and $\mathcal{M}^h$ be defined by* (54)*,* (55)*, and* (56)*, and let $B^h : \mathcal{U}^h \to \mathcal{M}^h$ be defined for every $V^h \in \mathcal{U}^h$ as*

$$\boldsymbol{\mu}^h_* = B^h(V^h) \Leftrightarrow (\boldsymbol{\mu}^h_*, \boldsymbol{\mu})_0 = (B(V^h), \boldsymbol{\mu})_0 \quad \forall \boldsymbol{\mu} \in \mathcal{M}^h. \tag{61}$$

*Then we have*

$$ker(B^h)^t = \{0\}. \tag{62}$$

*Proof.* From (61) we have immediately

$$ker(B^h)^t = \{\widetilde{\boldsymbol{\mu}} \in \mathcal{M}^h \text{ such that } (B(V^h), \widetilde{\boldsymbol{\mu}})_0 = 0 \; \forall \, V^h \in \mathcal{U}^h\} \tag{63}$$

and the result follows easily from Lemma 4.1. □

From Proposition 4.1 (plus (30) and known results) we have then existence and uniqueness of the solution of the discrete limit problem (59).

**Remark 4.2.** *It is worth noting that the proof of Proposition 4.1 works only because we are considering the case of a plate that is simply supported on the right and upper edges. On the other hand, the empty kernel property will not be true for a plate clamped all over* $\partial\Omega$. *Consider the case of a* $2 \times 2$ *grid, in which a checkerboard mode (in either one of the two components) can be easily seen to belong to* $ker(B^h)^t$. *However, as we are only interested in error estimates for* $U - U^h$, *our proofs can survive even in the case of a clamped plate by setting*

$$\mathcal{M}^h := \left(\mathcal{L}^{0,0}_{[r-1,r-1]}\right)_{/(ker(B^h)^t)}. \tag{64}$$

# 5 Error Estimates

Putting aside the problem of estimating $\boldsymbol{\lambda} - \boldsymbol{\lambda}^h$, we seek to estimate the distance between the solution $U \equiv (\boldsymbol{\theta}, w)$ of (58) and the solution $U^h \equiv (\boldsymbol{\theta}^h, w^h)$ of (59).

The following result is of a rather technical nature, and its proof will be given in Appendix B.

**Theorem 5.1.** *Let* $(U, \boldsymbol{\lambda}) \equiv ((\boldsymbol{\theta}, w), \boldsymbol{\lambda})$ *be the solution of* (58) *and* $r$ *an integer* $\geq 1$. *Let the spaces* $\boldsymbol{\Theta}^h$, $W^h$ *and* $\mathcal{M}^h$ *be defined as in* (54) *and* (55). *Assume that* $w \in H^{r+2}(\Omega)$. *Then there exist* $\widehat{\boldsymbol{\theta}} \in \boldsymbol{\Theta}^h$ *and* $\widehat{w} \in W^h$ *such that*

$$\|\boldsymbol{\theta} - \widehat{\boldsymbol{\theta}}\|_{(H_x, H_y)} \leq C \, h^r \, \|\boldsymbol{\theta}\|_{r+1,\Omega} \tag{65}$$

$$\|w - \widehat{w}\|_{1,\Omega} \leq C \, h^r \, \|w\|_{r+1,\Omega} \tag{66}$$

$$\int_R (w - \widehat{w})_{xy} \, v^h_{xy} \, dx \, dy \leq C h^r \|w\|_{r+2,\Omega} \, \|v^h\|_{H_{xy}} \quad \forall v^h \in W^h \tag{67}$$

$$(B(\widehat{\boldsymbol{\theta}}, \widehat{w}), \boldsymbol{\mu})_0 = 0 \quad \forall \boldsymbol{\mu} \in \mathcal{M}^h \tag{68}$$

Using Theorem 5.1 we can now prove the following error estimate

**Theorem 5.2.** *Let $(U,\boldsymbol{\lambda}) \equiv ((\boldsymbol{\theta},w),\boldsymbol{\lambda})$ be the solution of (58), let $r \geq 1$ be an integer, and let the spaces $\boldsymbol{\Theta}^h$, $W^h$ and $\mathcal{M}^h$ be defined as in (54) and (55). Let moreover $(U^h,\boldsymbol{\lambda}^h) \equiv ((\boldsymbol{\theta}^h,w^h),\boldsymbol{\lambda}^h)$ be the solution of (59). Then we have*

$$\|U^h - U\|_{\mathcal{U}} \leq C\, h^r \left(\|w\|_{r+2,\Omega} + \|\boldsymbol{\lambda}\|_{r,\Omega}\right) \tag{69}$$

*where $C$ is a constant independent of the decomposition.*

*Proof.* Let $\widehat{U} \equiv (\widehat{\boldsymbol{\theta}},\widehat{w})$ where $\widehat{\boldsymbol{\theta}}$ and $\widehat{w}$ are the functions given by Theorem 5.1. Using (30), and adding and subtracting $U$, we obtain

$$\begin{aligned} \alpha\|\widehat{U} - U^h\|_{\mathcal{U}}^2 &\leq \mathcal{A}_b(\widehat{U} - U^h, \widehat{U} - U^h) \\ &= \mathcal{A}_b(\widehat{U} - U, \widehat{U} - U^h) + \mathcal{A}_b(U - U^h, \widehat{U} - U^h). \end{aligned} \tag{70}$$

For the first term of (70), we use (67) to get

$$\begin{aligned} &\mathcal{A}_b(\widehat{U} - U, \widehat{U} - U^h) = \\ &\quad (\widehat{\theta}_{1,x} - \theta_{1,x}, \widehat{\theta}_{1,x} - \theta^h_{1,x})_0 + (\widehat{\theta}_{2,y} - \theta_{2,y}, \widehat{\theta}_{2,y} - \theta^h_{2,y})_0 + 2((\widehat{w} - w)_{xy}, (\widehat{w} - w^h)_{xy})_0 \\ &\qquad \leq C\left(\|\boldsymbol{\theta} - \widehat{\boldsymbol{\theta}}\|_{(Hx,Hy)} + h^r\|w\|_{r+2,\Omega}\right) \|\widehat{U} - U^h\|_{\mathcal{U}}. \end{aligned} \tag{71}$$

For the second term of (70), we use the first equations of (58) and (59) to get

$$\mathcal{A}_b(U - U^h, \widehat{U} - U^h) = (\boldsymbol{\lambda}^h, B(\widehat{U} - U^h))_0 - (\boldsymbol{\lambda}, B(\widehat{U} - U^h))_0 \tag{72}$$

and using the second equation of (59) and (68) we see that we can substitute $\boldsymbol{\lambda}^h$ with any other $\boldsymbol{\lambda}^I \in \mathcal{M}^h$ to get

$$\mathcal{A}_b(U - U^h, \widehat{U} - U^h) = (\boldsymbol{\lambda}^I - \boldsymbol{\lambda}, B(\widehat{U} - U^h))_0 \leq \|\boldsymbol{\lambda} - \boldsymbol{\lambda}^I\|_0 \, \|\widehat{U} - U^h\|_{\mathcal{U}}. \tag{73}$$

Hence we have

$$\|U^h - U\|_{\mathcal{U}} \leq C\left(\|\boldsymbol{\theta} - \widehat{\boldsymbol{\theta}}\|_{(Hx,Hy)} + \|\boldsymbol{\lambda} - \boldsymbol{\lambda}^I\|_0\right) + C\, h^r\|w\|_{r+2,\Omega} \tag{74}$$

with $C$ independent of the decomposition. Hence, taking $\boldsymbol{\lambda}^I$ as the $L^2$ projection of $\boldsymbol{\lambda}$ on $\mathcal{M}^h$, the result follows again from Theorem 5.1 and usual approximation properties. This concludes the proof. □

As is classical for the analysis of finite element approximations of the Reissner-Mindlin plate model, we also have $L^2$ error estimates for the twist-Kirchhoff model. For this, however, we have first to make a couple of observations. We observe that for the limit problems (58) and (59), we could introduce the *kernels*

$$\mathcal{K} := \{(\boldsymbol{\eta}, v) \in \mathcal{U} \text{ such that } \boldsymbol{\eta} = \nabla v\} \tag{75}$$

and

$$\mathcal{K}^h := \{(\boldsymbol{\eta}, v) \in \mathcal{U}^h \text{ such that } (\boldsymbol{\eta} - \nabla v, \boldsymbol{\mu}) = 0 \ \forall\, \boldsymbol{\mu} \in \mathcal{M}^h\}. \tag{76}$$

Let us then present $U$ and $U^h$ as solutions of the problems

$$\begin{cases} \text{find } U \in \mathcal{K} \text{ such that} \\ \mathcal{A}_b(U, V) = (G, V)_0 \quad \forall\, V \in \mathcal{K}, \end{cases} \tag{77}$$

and

$$\begin{cases} \text{find } U^h \in \mathcal{K}^h \text{ such that} \\ \mathcal{A}_b(U^h, V) = (G, V)_0 \quad \forall\, V \in \mathcal{K}^h \end{cases} \tag{78}$$

respectively. We point out that (77) and (78) can be seen as the variational formulations of the continuous and discrete problems associated with the Poisson-Kirchhoff model. We can now state and prove our $L^2$ estimate.

**Theorem 5.3.** *Let $U \equiv (\boldsymbol{\theta}, w) \in \mathcal{K}$ be the solution of (77). Let $r \geq 1$ be an integer, and let the spaces $\boldsymbol{\Theta}^h$, $W^h$ and $\mathcal{M}^h$ be defined as in (54) and (55). Moreover, let $U^h \equiv (\boldsymbol{\theta}^h, w^h) \in \mathcal{K}_h$ be the solution of (78). Then we have*

$$\|w^h - w\|_{0,\Omega} \leq C\, h^{r+1} \left( \|w\|_{r+2,\Omega} + \|\boldsymbol{\lambda}\|_{r,\Omega} \right) \tag{79}$$

*where $C$ is a constant independent of the decomposition.*

*Proof.* We start (as usual in the Aubin-Nitsche procedure) by considering the auxiliary problem

$$\begin{cases} \text{Find } Z \equiv (\boldsymbol{\varphi}, z) \in \mathcal{K} \text{ such that} \\ \mathcal{A}_b(V, Z) = (w^h - w, v)_0 \quad \forall\, V = (\boldsymbol{\eta}, v) \in \mathcal{K}. \end{cases} \tag{80}$$

We remark that $\mathcal{A}_b(V, Z) = \mathcal{A}_b(Z, V)$ and that $z$ will be the solution of a Poisson-Kirchhoff problem having $w^h - w$ as a distributed load. That is, we define $z$ to be the solution of the problem

$$\Delta^2 z = w_h - w \ \text{ in } \Omega, \tag{81}$$

with kinematic boundary conditions

$$z = 0 \ \text{ on } \partial\Omega, \qquad \varphi_1 \equiv z_x = 0 \text{ for } x = 0, \qquad \varphi_2 \equiv z_y = 0 \text{ for } y = 0, \tag{82}$$

and natural boundary conditions

$$\varphi_{1,x} \equiv z_{xx} = 0 \text{ for } x = L_1, \qquad \varphi_{2,y} \equiv z_{yy} = 0 \text{ for } y = L_2. \tag{83}$$

Using standard regularity theory we have:

$$\|z\|_{4,\Omega} \leq C\, \|w^h - w\|_{0,\Omega}. \tag{84}$$

Using (81), integration by parts, and the fact that $w - w^h = 0$ on $\partial\Omega$, we obtain

$$\begin{aligned} \|w^h - w\|^2_{0,\Omega} &= (w^h - w, \Delta^2 z)_0 \\ &= -\{((w^h - w)_x, z_{xxx})_0 + ((w^h - w)_y, z_{yyy})_0\} + 2((w^h - w)_{xy}, z_{xy})_0. \end{aligned} \tag{85}$$

At this point, we remark that, by adding and subtracting $\theta_1^h$ and noting that $w_x = \theta_1$:

$$((w^h - w)_x, z_{xxx})_0 = (w_x^h - \theta_1^h, z_{xxx})_0 + (\theta_1^h - \theta_1, z_{xxx})_0. \tag{86}$$

Let us take $\mu \in \mathcal{L}^{0,0}_{[0,0]}$ to be the $L^2$-projection of $z_{xxx}$ onto $\mathcal{L}^{0,0}_{[0,0]}$, the space of piecewise constants. Since $U^h \in \mathcal{K}_h$ we have, using (76), the Cauchy-Schwarz inequality, usual approximation estimates, the equality $w_x \equiv \theta_1$, and (84):

$$\begin{aligned}(w_x^h - \theta_1^h, z_{xxx})_0 &= (w_x^h - \theta_1^h, z_{xxx} - \mu)_0 \leq \|w_x^h - \theta_1^h\|_{0,\Omega}\, C\, h \|z_{xxx}\|_{H^1(\Omega)} \\ &\leq \big(\|w_x^h - w_x\|_{0,\Omega} + \|\theta_1 - \theta_1^h\|_{0,\Omega}\big)\, C\, h \|z_{xxx}\|_{H^1(\Omega)} \\ &\leq C\, h\, \|U^h - U\|_{\mathcal{U}} \|z\|_{4,\Omega} \leq C\, h\, \|U^h - U\|_{\mathcal{U}} \|w^h - w\|_{0,\Omega}.\end{aligned} \tag{87}$$

Collecting (85)-(87) and the counterparts of (86)-(87) for the quantities $(w^h - w)_y$ and $w_y^h - \theta_2^h$, we obtain

$$\|w^h - w\|^2_{0,\Omega} = -\{(\theta_1^h - \theta_1, z_{xxx})_0 + (\theta_2^h - \theta_2, z_{yyy})_0\} + 2((w^h - w)_{xy}, z_{xy})_0 + E \tag{88}$$

where

$$|E| \leq C\, h\, \|U^h - U\|_{\mathcal{U}} \|w^h - w\|_{0,\Omega}. \tag{89}$$

Now let us recall $\theta_1^h - \theta_1 = 0$ for $x = 0$, $\boldsymbol{\varphi} \equiv \nabla z$, and the boundary conditions (82) and (83). Integrating by parts we obtain:

$$(\theta_1^h - \theta_1, z_{xxx})_0 = (\theta_1^h - \theta_1, \varphi_{1,xx})_0 = -((\theta_1^h - \theta_1)_x, \varphi_{1,x})_0. \tag{90}$$

Inserting the above expression into (88) (and inserting a similar expression for the second component) gives

$$\begin{aligned}\|w^h - w\|^2_{0,\Omega} &= ((\theta_1^h - \theta_1)_x, \varphi_{1,x})_0 + ((\theta_2^h - \theta_2)_y, \varphi_{2,y})_0 + 2((w^h - w)_{xy}, z_{xy})_0 + E \\ &= \mathcal{A}_b(U^h - U, Z) + E.\end{aligned} \tag{91}$$

Using (77), (78), Theorem 5.1, (84), and (89) we have

$$\begin{aligned}\|w^h - w\|^2_{0,\Omega} &= \mathcal{A}_b(U^h - U, Z) + E = \mathcal{A}_b(U^h - U, Z - \hat{Z}) + E \\ &\leq \|U^h - U\|_{\mathcal{U}}\, C\, h \|z\|_{4,\Omega} + |E| \leq C\, h\, \|U^h - U\|_{\mathcal{U}} \|w^h - w\|_{0,\Omega}\end{aligned} \tag{92}$$

and the desired estimate follows easily from the previous estimate (69). □

**Remark 5.1.** *In the lowest order case Theorem 5.2 provides first order convergence in $L^2(\Omega)$ for all the variables: $\boldsymbol{\theta}$, $\theta_{1,x}$, $\theta_{2,y}$, $w$, $w_x$, $w_y$, and $w_{xy}$, while Theorem 5.3 provides second order convergence for $w$ in $L^2(\Omega)$.*

# 6 Numerical Results

We now present numerical results using our new plate element and the twist-Kirchhoff theory. It should be noted that while the multiplier formulation was utilized to obtain theoretical results, in practice, one needs not actually compute using Lagrange multipliers. Instead, one may equivalently utilize the primal formulation in conjunction with a reduced quadrature rule. For the $r^{th}$-order plate element, one uses an $r \times r$-point tensor-product Gaussian quadrature rule. For the first-order element this, as we have seen, corresponds to a one-point quadrature rule. The results obtained in this section were obtained using the reduced quadrature approach.

## 6.1 Comparison with an Exact Solution

We begin the numerical results section by analyzing the effectiveness of the new plate element in simulating a model problem with a known exact solution. We consider the model problem given by (32) and equipped with simply-supported boundary conditions on all four sides of the rectangular plate. Through integration by parts, we find the strong form of this problem takes the following form: find $w$ and $\boldsymbol{\theta}$ such that

$$\begin{aligned}
-\theta_{1,xx} - t^{-2}\left(w_x - \theta_1\right) &= 0 \quad \text{in } \Omega && (93)\\
-\theta_{2,yy} - t^{-2}\left(w_y - \theta_2\right) &= 0 \quad \text{in } \Omega && (94)\\
2w_{xxyy} - t^{-2}\left(w_{xx} + w_{yy} - \theta_{1,x} - \theta_{2,y}\right) &= g \quad \text{in } \Omega && (95)\\
w &= 0 \quad \text{on } \partial\Omega && (96)\\
\theta_{1,x} n_x + \theta_{2,y} n_y &= 0 \quad \text{on } \partial\Omega && (97)\\
& && (98)
\end{aligned}$$

where $\mathbf{n} = (n_x, n_y)$ denotes the outward-pointing unit normal to $\Omega$. One sees that (93) and (94) represent the equations of moment equilibrium for the model twist-Kirchhoff plate, (95) represents the transverse equilibrium equation, and (96) and (97) correspond to the simply-supported boundary conditions (zero displacement and zero normal moment). If the length of the sides of the rectangle are taken to be unity (i.e., $L_1 = L_2 = 1$) and the load $g$ is given as

$$g = \pi^4\left(4 + 2\pi^2 t^2\right)\sin(\pi x)\sin(\pi y) \tag{99}$$

then it is easily verified that the exact solution to (93)-(97) is

$$\begin{aligned}
w &= \left(1 + \pi^2 t^2\right)\sin(\pi x)\sin(\pi y) && (100)\\
\boldsymbol{\theta} &= \left(\pi\cos(\pi x)\sin(\pi y), \pi\sin(\pi x)\cos(\pi y)\right). && (101)
\end{aligned}$$

To analyze the effectiveness of the proposed twist-Kirchhoff plate elements, we computed discrete solutions for the first- and second-order cases and thickness values of 0.01, 0.001, and 0.0001 and then compared these solutions to the exact solution. In Figure 2, we present the error as measured by the total norm $\|\cdot\|_{\mathcal{U}}$, that is, the norm defined by (23).

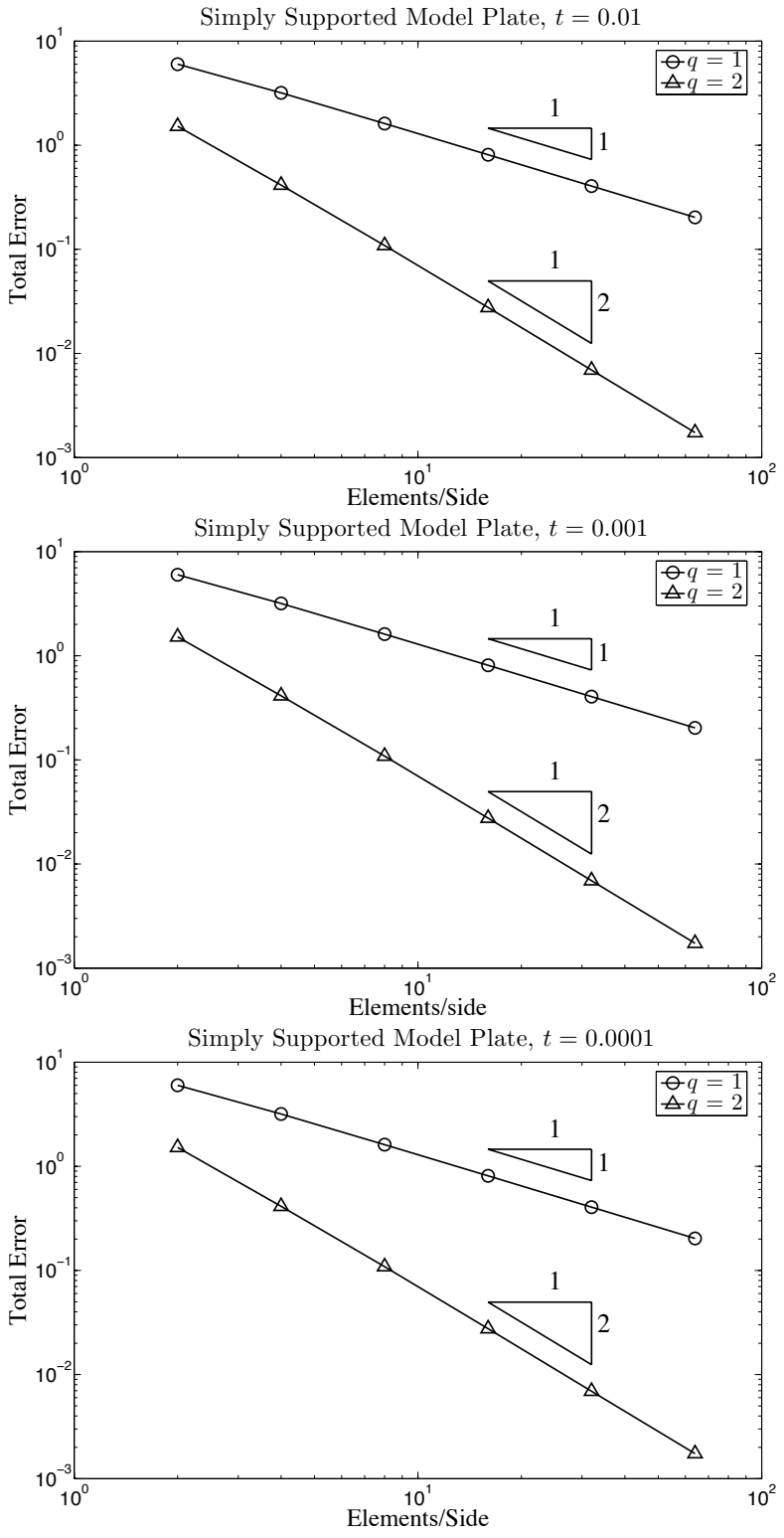


Figure 2: The total error (as measured by the total norm $\|\cdot\|_{\mathcal{U}}$) induced by the first- and second-order plate elements for the simply-supported model plate problem and thickness values of 0.01, 0.001, and 0.0001.

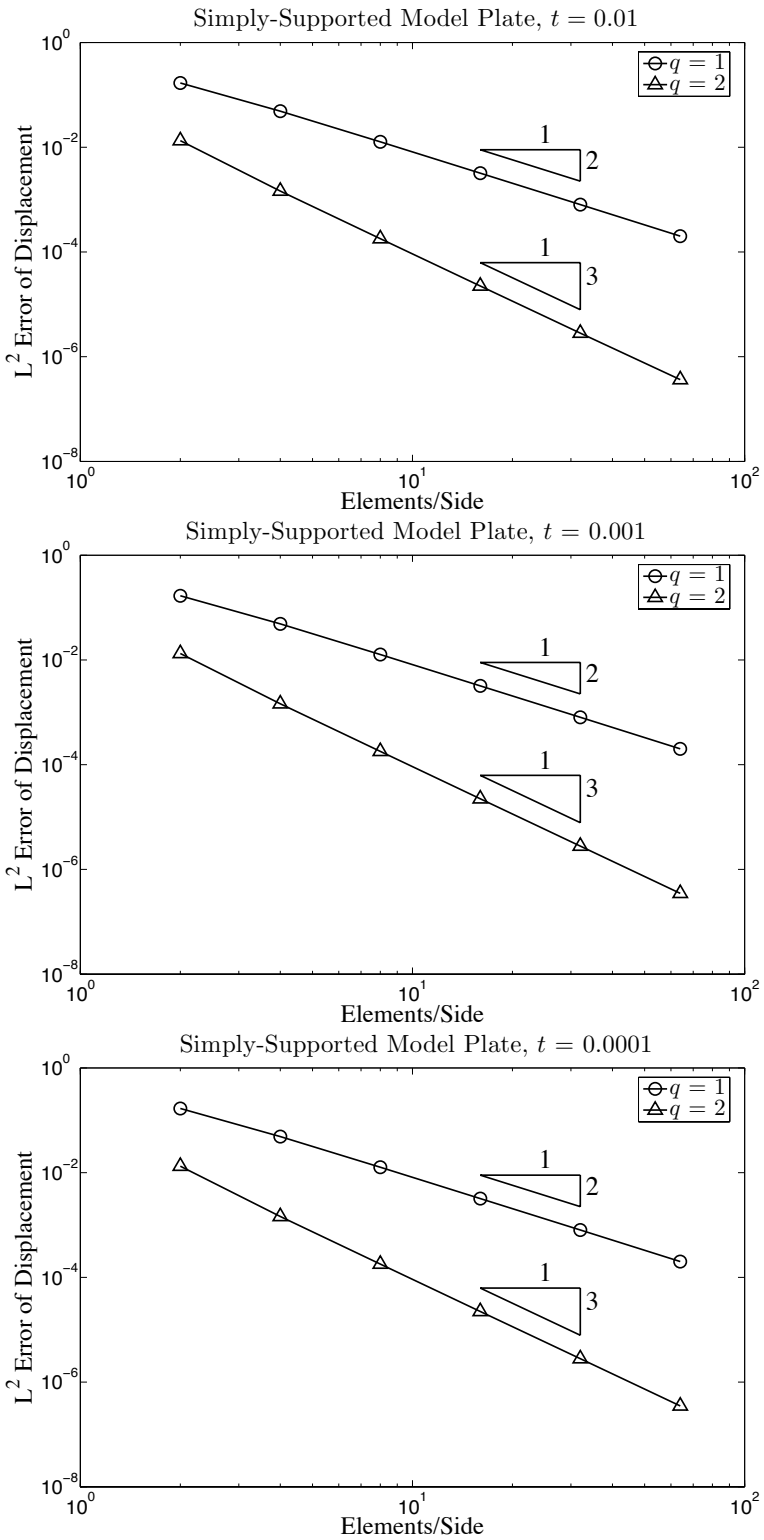


Figure 3: The displacement error (as measured by the $L^2$ norm) induced by the first- and second-order plate elements for the simply-supported model plate problem and thickness values of 0.01, 0.001, and 0.0001.

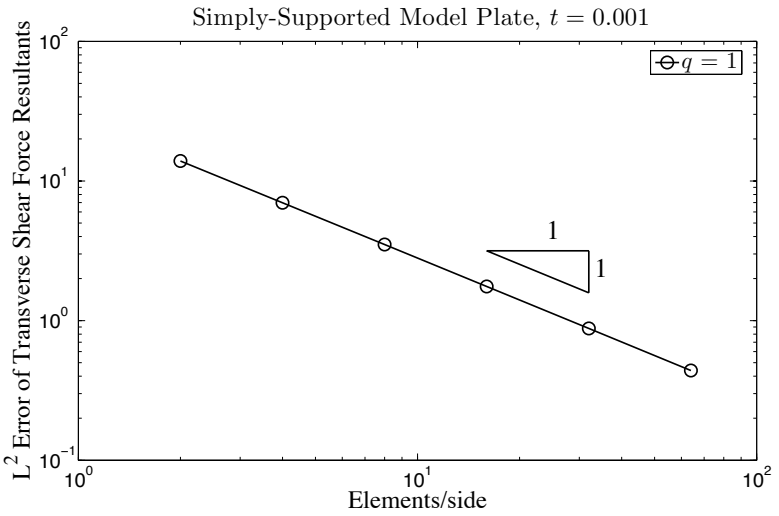


Figure 4: The transverse shear force resultant error (as measured by the $L^2$ norm) induced by the first-order plate element for the simply-supported model plate problem and a thickness value of 0.001.

Analyzing the figure, we confirm the theoretical rates of convergence given by Theorem 5.2. Further, we observe no locking as the thickness/width ratio is decreased.

In Figure 3, we present the error of the displacements as measured by the $L^2$ norm. Analyzing the figure, we confirm the theoretical rates of convergence given by Theorem 5.3. Further, as before, we observe no locking as the thickness/width ratio is decreased. In Figure 4, we present the error of the discrete transverse shear force resultant for the first-order element, taken to be element-wise constant and obtained by sampling the resultant $t^{-2}\left(\nabla w^h - \boldsymbol{\theta}^h\right)$ at element centers, as measured by the $L^2$ norm. We observe that a linear convergence rate is obtained.

**Remark 6.1.** *Note that in the twist-Kirchhoff theory, the vhoice of boundary conditions is identical to that of Poisson-Kirchhoff theory. Notably, we do not have enough freedom (or regularity) to impose boundary conditions for the tangential component of the rotation or moment vectors. Thus, we are restricted to Kirchhoff-type simply-supported ($w = 0, M_n = 0$) and clamped ($w = 0, \theta_n = 0$) boundaries rather than the "hard" and "soft" boundaries associated with Reissner-Mindlin plates.*

## 6.2 Simply-Supported Isotropic Square Plate

We now consider the problem of a simply-supported isotropic square plate subject to uniform loading. For this problem, the forcing function is taken to be

$$g = \frac{1}{\mu t^3} q \tag{102}$$

where $\mu$ is given by (40) and $q$ is a uniform loading per unit area. Other details for a general isotropic twist-Kirchhoff plate, such as the bending part of the bilinear form, are presented in Remark 2.2. For all subsequent computations, a shear correction factor of 5/6 is utilized to achieve results that are consistent with classical bending theory [18].

We first study convergence rates. Since there is no known analytical solution to the twist-Kirchhoff problem, we compare discrete solutions with a heavily refined ($128^2$ elements) second-order solution which can be considered to be approximately exact. In Figure 5(a), we present the total error as measured by the norm $\|\cdot\|_{\mathcal{U}}$ for $q = 1$ and a square plate with width $a = 1$, thickness $t = 0.001$, Young's modulus $E = 10^7$, and Poisson's ratio $\nu = 0.3$. Similarly, we present the displacement error as measured by the $L^2$ norm in Figure 5(b). The plotted errors are normalized by the norms of the exact solution. Analyzing these figures, we observe optimal rates of convergence for the first- and second-order cases. We have tested for other material parameters and thickness/width ratios and found similar convergence behavior and no locking phenomena.

We now study the convergence of the center displacement. Tables 1 and 2 display the convergence of the center displacement for the first- and second-order plate elements respectively. The displayed center displacements are scaled by $10^3 D/\left(qa^4\right)$ where

$$D = \frac{Et^3}{12(1-\nu^2)} \tag{103}$$

is the plate stiffness. We note that the center displacement converges for both the first- and second-order cases, with the second-order discretization converging faster. In fact, for a mesh of $32^2$ elements, the center displacement for the second-order discretization has already converged to six significant figures. In addition, we observe no locking phenomena. Comparing our converged twist-Kirchhoff results with the reference Poisson-Kirchhoff solution [25][2], we find the twist-Kirchhoff center displacement converges to the thin plate displacement from above as the thickness/width ratio $t/a \to 0$. This is consistent with the behavior of Reissner-Mindlin plates. To compare our twist-Kirchhoff results with Reissner-Mindlin theory, we have simulated a soft simply-supported Reissner-Mindlin plate using $256^2$ quadratic Lagrange elements and selective reduced integration [19]. Table 3 displays the computed center displacements, which we have confirmed are converged to five significant digits. We find the converged twist-Kirchhoff displacements lie below the corresponding Reissner-Mindlin displacements for a fixed thickness/width ratio $t/a$. This result seems consistent with the "in between" nature of the twist-Kichhoff theory.

We next study the convergence of the center bending moment about the $x$-axis. That is, we study convergence of the quantity

$$M_x = -\sum_{1\le\gamma,\delta\le 2} c_{11\gamma\beta}\kappa_{\gamma\beta} \tag{104}$$

at the center of the plate where

$$c_{\alpha\beta\gamma\delta} = t^3 A_{\alpha\beta\gamma\delta} \tag{105}$$

[2]The center displacement of the Poisson-Kirchhoff plate is given by a rapidly converging series in Chapter 5 of [25]. In our comparison, we used enough terms to obtain a solution accurate to six significant digits.

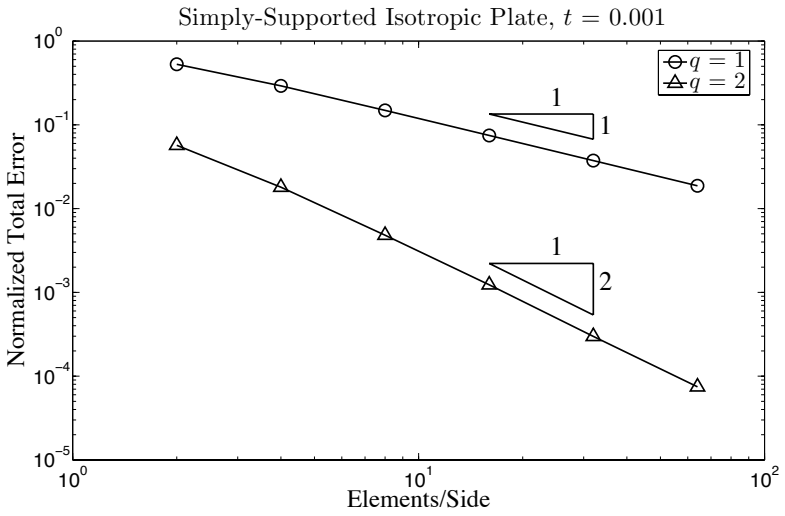


(a)

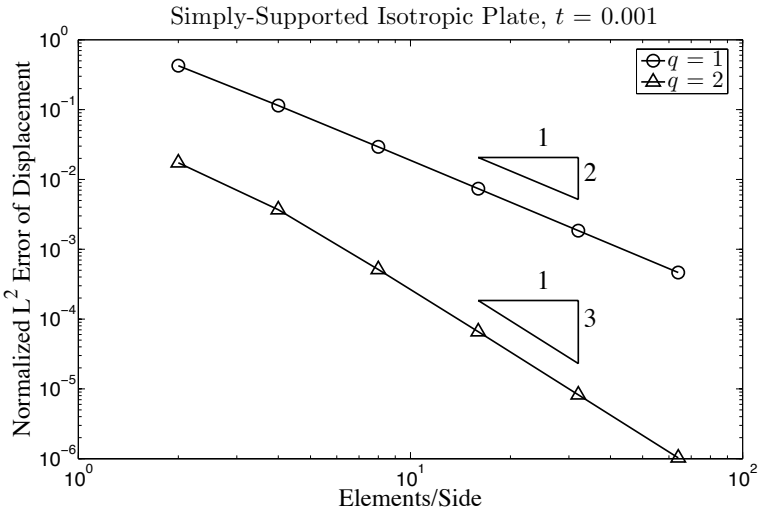


(b)

Figure 5: (a) The normalized total error produced by the lowest- and second-order plate elements for the simply-supported isotropic plate under a uniform load for a thickness value of 0.001. (b) The normalized $L^2$ norm of the displacement for the same problem.

| $n_{el}$ | $t/a = 0.05$ | $t/a = 0.01$ | $t/a = 0.001$ | $t/a = 0.0001$ |
|---|---|---|---|---|
| $2^2$ | 3.94378 | 3.90776 | 3.90627 | 3.90625 |
| $4^2$ | 4.14448 | 4.12412 | 4.12327 | 4.12326 |
| $8^2$ | 4.09722 | 4.07794 | 4.07714 | 4.07714 |
| $16^2$ | 4.08594 | 4.06677 | 4.06597 | 4.06597 |
| $32^2$ | 4.08318 | 4.06405 | 4.06326 | 4.06325 |
| $64^2$ | 4.08250 | 4.06338 | 4.06259 | 4.06258 |

Table 1: Center displacement ($w \times 10^3 D/(qa^4)$) for first-order element simply-supported square plate solutions with uniform loading for various thickness/length ratios. Reference thin plate limit solution is 4.06235 [25].

| $n_{el}$ | $t/a = 0.05$ | $t/a = 0.01$ | $t/a = 0.001$ | $t/a = 0.0001$ |
|---|---|---|---|---|
| $2^2$ | 4.23636 | 4.21946 | 4.21876 | 4.21875 |
| $4^2$ | 4.09021 | 4.07126 | 4.07048 | 4.07047 |
| $8^2$ | 4.08274 | 4.06363 | 4.06284 | 4.06283 |
| $16^2$ | 4.08230 | 4.06318 | 4.06239 | 4.06239 |
| $32^2$ | 4.08227 | 4.06315 | 4.06236 | 4.06236 |
| $64^2$ | 4.08227 | 4.06315 | 4.06236 | 4.06236 |

Table 2: Center displacement ($w \times 10^3 D/(qa^4)$) for second-order element simply-supported square plate solutions with uniform loading for various thickness/length ratios. Reference thin plate limit solution is 4.06235 [25].

| $t/a = 0.05$ | $t/a = 0.01$ | $t/a = 0.001$ | $t/a = 0.0001$ |
|---|---|---|---|
| 4.28955 | 4.09930 | 4.06585 | 4.06268 |

Table 3: Center displacement ($w \times 10^3 D/(qa^4)$) for soft simply-supported Reissner-Mindlin plate. Computed using $256^2$ quadratic Lagrange elements and selective reduced integration [19].

and $A_{\alpha\beta\gamma\delta}$ and $\kappa_{\gamma\beta}$ are defined by (36) and (37) respectively. Since the discrete center bending moment is not well-defined, we sample the discrete bending moment at a quadrature point lying closest to the center of the plate (the moment is equal at all quadrature points lying closest to the center of the plate due to symmetry). For the lowest-order element, the moment is constant within the element, whereas for the for the second-order element, the moment at the $2 \times 2$ Gauss point nearest the center of the plate is studied. Tables 4 and 5 display the convergence of the center moments for the first- and second-order plate elements respectively for a Poisson's ratio of $\nu = 0.3$. The displayed center moments are scaled by $10^2/(qa^2)$. We note that the bending moment converges for both the first- and second-order cases, with the second-order discretization

| $n_{el}$ | $t/a = 0.05$ | $t/a = 0.01$ | $t/a = 0.001$ | $t/a = 0.0001$ |
|---|---|---|---|---|
| $2^2$ | 2.02074 | 2.03083 | 2.03125 | 2.03125 |
| $4^2$ | 4.21661 | 4.23116 | 4.23176 | 4.23177 |
| $8^2$ | 4.63751 | 4.65186 | 4.65245 | 4.65246 |
| $16^2$ | 4.73991 | 4.75403 | 4.75462 | 4.75462 |
| $32^2$ | 4.76547 | 4.77955 | 4.78013 | 4.78014 |
| $64^2$ | 4.77185 | 4.78592 | 4.78651 | 4.78651 |

Table 4: "Center" bending moment about the $x$-axis ($M_x \times 10^2/(qa^2)$) for first-order element simply-supported square plate solutions with uniform loading for various thickness/length ratios and a Poisson's ratio of $\nu = 0.3$. Numerical value of "center" bending moment is taken at the $1 \times 1$ Gauss quadrature point nearest the center of the plate. Reference thin plate limit solution is 4.78864 [25].

| $n_{el}$ | $t/a = 0.05$ | $t/a = 0.01$ | $t/a = 0.001$ | $t/a = 0.0001$ |
|---|---|---|---|---|
| $2^2$ | 4.56984 | 4.58412 | 4.58472 | 4.58472 |
| $4^2$ | 4.69254 | 4.70651 | 4.70709 | 4.70709 |
| $8^2$ | 4.75191 | 4.76593 | 4.76651 | 4.76651 |
| $16^2$ | 4.76836 | 4.78241 | 4.78300 | 4.78301 |
| $32^2$ | 4.77257 | 4.78663 | 4.78722 | 4.78723 |
| $64^2$ | 4.77363 | 4.78770 | 4.78828 | 4.78831 |

Table 5: "Center" bending moment about the $x$-axis ($M_x \times 10^2/(qa^2)$) for second-order element simply-supported square plate solutions with uniform loading for various thickness/length ratios and a Poisson's ratio of $\nu = 0.3$. Numerical value of "center" bending moment is taken at the $2 \times 2$ Gauss quadrature point nearest the center of the plate. Reference thin plate limit solution is 4.78864 [25].

converging faster, and we observe no locking phenomena. As expected, the convergence rate for the bending moment is slower than that for the center displacement. Comparing our converged twist-Kirchhoff results with the reference converged Poisson-Kirchhoff solution [25][3], we find the twist-Kirchhoff center bending moment converges to the thin plate moment from below as the thickness/width ratio $t/a \to 0$.

For all of the computations here, the full twist-Kirchhoff plate was modeled. In addition, we have run computations where a quarter of the full plate is modeled instead and symmetry boundary conditions are employed. As expected, we obtain identical results using this strategy.

[3]The center moment of the Poisson-Kirchhoff plate is given by a rapidly converging series in Chapter 5 of [25]. In our comparison, we used enough terms to obtain a solution accurate to six significant digits.

## 6.3 Fully Clamped Isotropic Square Plate

We finish the numerical results section by considering the problem of a fully clamped isotropic square plate subject to uniform loading. As was the case for the simply-supported isotropic plate, a shear correction factor of 5/6 is utilized to achieve results that are consistent with classical bending theory.

We first study convergence rates. As before, we compare discrete solutions with a heavily refined ($128^2$ elements) second-order solution which can be considered to be approximately exact. In Figure 6(a), we present the total error as measured by the norm $\|\cdot\|_{\mathcal{U}}$ for $q = 1$ and a square plate with width $a = 1$, thickness $t = 0.001$, Young's modulus $E = 10^7$, and Poisson's ratio $\nu = 0.3$. Similarly, we present the displacement error as measured by the $L^2$ norm in Figure 6(b). The plotted errors are normalized by the norms of the exact solution. Analyzing these figures, we observe optimal rates of convergence for the first- and second-order cases. We have tested for other material parameters and thickness/width ratios and found similar convergence behavior and no locking phenomena.

We now study the convergence of the center displacement. Tables 6 and 7 display the convergence of the center displacement for the first- and second-order plate elements respectively. The displayed center displacements are again scaled by $10^3 D/\left(qa^4\right)$. We note that the center displacement converges for both the first- and second-order cases, with the second-order discretization converging faster, and we observe no locking phenomena. Comparing our converged twist-Kirchhoff results with the reference Poisson-Kirchhoff solution [24], we find the twist-Kirchhoff center displacement converges to the thin plate displacement from above as the thickness/width ratio $t/a \to 0$. To compare our twist-Kirchhoff results with Reissner-Mindlin theory, we have simulated a soft clamped Reissner-Mindlin plate using $256^2$ quadratic Lagrange elements and selective reduced integration [19]. Table 8 displays the computed center displacements, which we have confirmed are converged to six significant digits. As was the case for the simply-supported plate, we find the converged twist-Kirchhoff displacements lie below the corresponding Reissner-Mindlin displacements for a fixed thickness/width ratio $t/a$. This result again seems consistent with the "in between" nature of the twist-Kichhoff theory.

We next study the convergence of the center bending moment about the $x$-axis. As was done for the simply-supported case, we sample the discrete bending moment at a quadrature point lying closest to the center of the plate. Tables 9 and 10 display the convergence of the center displacement for the first- and second-order plate elements respectively for a Poisson's ratio of $\nu = 0.3$. The displayed center moments are scaled by $10^2/\left(qa^2\right)$. We note that the bending moment converges for both the first- and second-order cases, with the second-order discretization converging faster, and we observe no locking phenomena. Comparing our converged twist-Kirchhoff results with the reference converged Poisson-Kirchhoff solution [24], we find the twist-Kirchhoff center bending moment converges to the thin plate moment from below as the thickness/width ratio $t/a \to 0$.

As was the case for the simply-supported plate, the full twist-Kirchhoff plate was modeled for all the computations here. We have run computations using a quarter plate

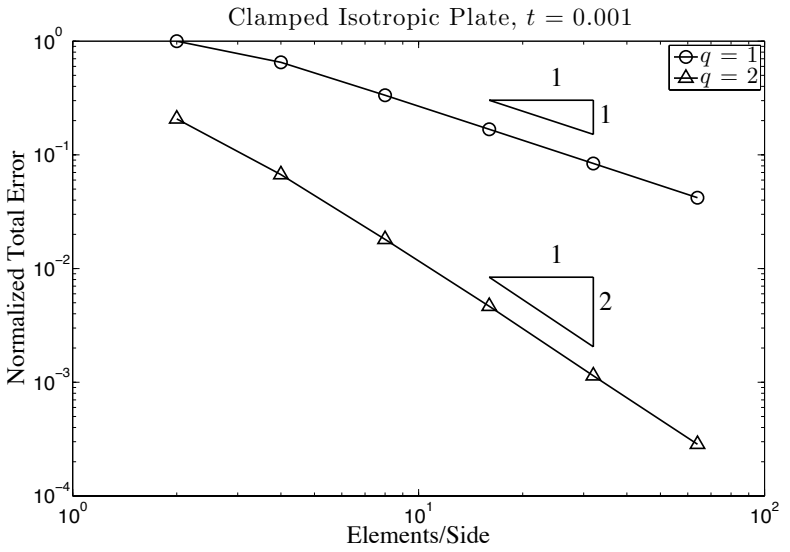


(a)

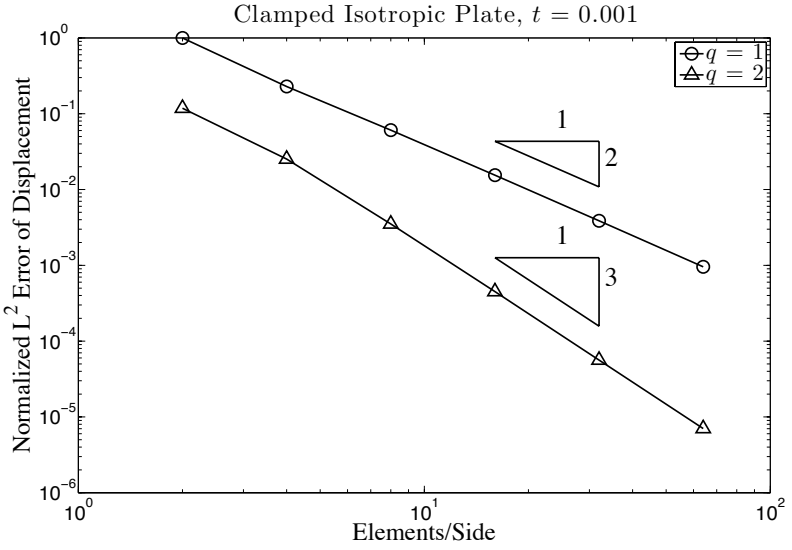


(b)

Figure 6: (a) The normalized total error produced by the lowest- and second-order plate elements for the fully clamped isotropic plate under a uniform load for a thickness value of 0.001. (b) The normalized $L^2$ norm of the displacement for the same problem.

| $n_{el}$ | $t/a = 0.05$ | $t/a = 0.01$ | $t/a = 0.001$ | $t/a = 0.0001$ |
|---|---|---|---|---|
| $2^2$ | 0.0885771 | 0.00357029 | 3.57142e-05 | 3.57143e-07 |
| $4^2$ | 1.34010 | 1.30355 | 1.30210 | 1.30208 |
| $8^2$ | 1.31588 | 1.27353 | 1.27177 | 1.27175 |
| $16^2$ | 1.31091 | 1.26862 | 1.26686 | 1.26684 |
| $32^2$ | 1.30976 | 1.26747 | 1.26571 | 1.26569 |
| $64^2$ | 1.30948 | 1.26719 | 1.26543 | 1.26541 |

Table 6: Center displacement ($w \times 10^3 D/(qa^4)$) for first-order element clamped square plate solutions with uniform loading for various thickness/length ratios. Reference thin plate limit solution is 1.26532 [24].

| $n_{el}$ | $t/a = 0.05$ | $t/a = 0.01$ | $t/a = 0.001$ | $t/a = 0.0001$ |
|---|---|---|---|---|
| $2^2$ | 1.59240 | 1.56365 | 1.56251 | 1.56250 |
| $4^2$ | 1.32290 | 1.28087 | 1.27912 | 1.27910 |
| $8^2$ | 1.31019 | 1.26792 | 1.26616 | 1.26615 |
| $16^2$ | 1.30944 | 1.26715 | 1.26539 | 1.26537 |
| $32^2$ | 1.30939 | 1.26710 | 1.26534 | 1.26532 |
| $64^2$ | 1.30939 | 1.26710 | 1.26534 | 1.26532 |

Table 7: Center displacement ($w \times 10^3 D/(qa^4)$) for second-order element clamped square plate solutions with uniform loading for various thickness/length ratios. Reference thin plate limit solution is 1.26532 [24].

| $t/a = 0.05$ | $t/a = 0.01$ | $t/a = 0.001$ | $t/a = 0.0001$ |
|---|---|---|---|
| 1.32856 | 1.26787 | 1.26534 | 1.26532 |

Table 8: Center displacement ($w \times 10^3 D/(qa^4)$) for soft clamped Reissner-Mindlin plate. Computed using $256^2$ quadratic Lagrange elements and selective reduced integration [19].

instead and symmetry boundary conditions and obtained identical results.

# 7 Conclusions and Future Directions

We have presented a new theory of thin plates, the "twist-Kirchhoff theory," in which the twist component of curvature is computed by invoking the Kirchhoff hypothesis, while the direct components of curvature are computed from the rotations, as in Reissner-Mindlin theory. The theory lies in between the Poisson-Kirchhoff theory of thin plates, in which transverse shear strains are assumed identically zero, and the Reissner-Mindlin theory of shear-deformable plates. The twist component of curvature is not invariant

| $n_{el}$ | $t/a = 0.05$ | $t/a = 0.01$ | $t/a = 0.001$ | $t/a = 0.0001$ |
|---|---|---|---|---|
| $2^2$ | 0 | 0 | 0 | 0 |
| $4^2$ | 2.01757 | 2.03069 | 2.03124 | 2.03125 |
| $8^2$ | 2.22451 | 2.23235 | 2.23266 | 2.23266 |
| $16^2$ | 2.26901 | 2.27610 | 2.27639 | 2.27639 |
| $32^2$ | 2.27987 | 2.28670 | 2.28698 | 2.28699 |
| $64^2$ | 2.28258 | 2.28935 | 2.28963 | 2.28963 |

Table 9: "Center" bending moment about the $x$-axis ($M_x \times 10^2/(qa^2)$) for first-order element clamped square plate solutions with uniform loading for various thickness/length ratios and a Poisson's ratio of $\nu = 0.3$. Numerical value of "center" bending moment is taken at the $1 \times 1$ Gauss quadrature point nearest the center of the plate. Reference thin plate limit solution is 2.29051 [24].

| $n_{el}$ | $t/a = 0.05$ | $t/a = 0.01$ | $t/a = 0.001$ | $t/a = 0.0001$ |
|---|---|---|---|---|
| $2^2$ | 2.20857 | 2.21934 | 2.21979 | 2.21979 |
| $4^2$ | 2.20993 | 2.21628 | 2.21654 | 2.21654 |
| $8^2$ | 2.26197 | 2.26862 | 2.26889 | 2.26889 |
| $16^2$ | 2.27791 | 2.28463 | 2.28490 | 2.28491 |
| $32^2$ | 2.28208 | 2.28882 | 2.28909 | 2.28910 |
| $64^2$ | 2.28313 | 2.28988 | 2.29015 | 2.29016 |

Table 10: "Center" bending moment about the $x$-axis ($M_x \times 10^2/(qa^2)$) for second-order element clamped square plate solutions with uniform loading for various thickness/length ratios and a Poisson's ratio of $\nu = 0.3$. Numerical value of "center" bending moment is taken at the $2 \times 2$ Gauss quadrature point nearest the center of the plate. Reference thin plate limit solution is 2.29051 [24].

under global coordinate rotations, consequently neither is the theory. However, it is suitable for the development of plate elements in which we work in a preferential, local coordinate system. In fact, it provides a natural setting in which we may take advantage of Raviart-Thomas interpolations for rotations in combination with standard Lagrange interpolations for transverse displacement to form stable and convergent approximations of all orders. The lowest-order rectangular element, possessing four vertex transverse displacement degrees of freedom and four mid-side rotation degrees of freedom, eight in all, allows exact evaluation of the stiffness matrix with one-point Gaussian quadrature and is, in our opinion, the simplest effective rectangular element ever developed.

Three distinct directions of research present themselves. The first is, of course, generalization to the arbitrary quadrilateral element case. The second research direction is to adopt the framework of Isogeometric Analysis [13, 20] and develop smooth spline generalizations of the $C^0$-continuous finite elements described herein. We note that recent progress on the generalization of Raviart-Thomas interpolations to smooth B-splines and

NURBS in the context of electromagnetic [11] and fluid flow [10] problems suggests the significant potential of this development. The third direction is the search for membrane element discretizations that complement the new plate elements. The objective would be to create stable and convergent membrane elements that utilize the same quadrature rules as the corresponding bending elements. A key prize would be a one-point quadrature, four-node shell element, with mid-side rotation degrees of freedom, sixteen in all, devoid of hourglass modes. Such an element would have the potential to revolutionize crash dynamics and many sheet metal forming applications. The search for better tools goes on and it seems is never ending.

# Acknowledgements

F. Brezzi and L.D. Marini were partially supported by the Italian Ministry of Education (MIUR) through the program PRIN 2008. J.A. Evans was partially supported by the Department of Energy Computational Science Graduate Fellowship, provided under grant number DE-FG02-97ER25308. T.J.R. Hughes was partially supported by the Office of Naval Research under Contract No. N00014-08-0992 and by the National Science Foundation under Grant No. 0700204. This support is gratefully acknowledged.

# References

[1] J H Argyris, I Fried, and D W Scharpf. The TUBA family of plate elements for the matrix displacement method. *The Aeronautical Journal of the Royal Aeronautical Society*, 72:701–709, 1968.

[2] K J Bathe, F Brezzi, and L D Marini. The MITC9 shell element in plate bending: Mathematical analysis of a simplified case. *Computational Mechanics*, 2010. In press.

[3] Y Bazilevs, L Beirao da Veiga, J A Cottrell, T J R Hughes, and G Sangalli. Isogeometric analysis: Approximation, stability and error estimates for $h$-refined meshes. *Mathematical Models and Methods in Applied Sciences*, 16:1–60, 2006.

[4] K Bell. A refined triangular plate bending finite element. *International Journal for Numerical Methods in Engineering*, 1:101–122, 1969.

[5] T Belytschko, J I Lin, and C S Tsay. Explicit algorithms for nonlinear dynamics of shells. *Computer Methods in Applied Mechanics and Engineering*, 42:225–251, 1984.

[6] T Belytschko and C S Tsay. A stabilization procedure for the quadrilateral plate element with one-point quadrature. *International Journal for Numerical Methods in Engineering*, 19:405–419, 1983.

[7] F Brezzi, K J Bathe, and M Fortin. Mixed-interpolated elements for Reissner-Mindlin plates. *International Journal for Numerical Methods in Engineering*, 28:1787–1801, 1989.

[8] F Brezzi and M Fortin. *Mixed and Hybrid Finite Element Methods*. Springer-Verlag New York, Inc., New York, NY, 1991.

[9] F Brezzi, M Fortin, and R Stenberg. Error analysis of mixed-interpolated elements for Reissner-Mindlin plates. *Mathematical Models and Methods in Applied Sciences*, 1:125–151, 1991.

[10] A Buffa, C de Falco, and G Sangalli. Isogeometric analysis: Stable elements for the 2D Stokes equation. *International Journal for Numerical Methods in Fluids*, 2010. Published online. DOI: 10.1002/fld.2337.

[11] A Buffa, G Sangalli, and R Vázquez. Isogeometric analysis in electromagnetics: B-splines approximation. *Computer Methods in Applied Mechanics and Engineering*, 199:1143–1152, 2010.

[12] R W Clough and J L Tocher. Finite element stiffness matrices for analysis of plate bending. In *Proceedings of the Conference on Matrix Methods in Structural Mechanics*, pages 515–545, Wright-Patterson Air Force Base, Ohio, 1965.

[13] J A Cottrell, T J R Hughes, and Y Bazilevs. *Isogeometric Analysis: Toward Integration of CAD and FEA*. Wiley, Chichester, UK, 2009.

[14] G R Cowper, E Kosko, G M Lindeberg, and M D Olson. A high precision triangular plate bending element. Technical Report Aeronautical Report. LR-5 14, National Research Council of Canada, December 1968.

[15] B Fraeijs de Veubeke. A conforming finite element for plate bending. *International Journal of Solids and Structures*, 4:95–108, 1967.

[16] R S Falk. Finite elements for the Reissner-Mindlin plate. *Lecture Notes in Mathematics*, 1939:195–232, 2008.

[17] D P Flanagan and T Belytschko. A uniform strain hexahedron and quadrilateral with orthogonal hourglass control. *International Journal for Numerical Methods in Engineering*, 17:679–706, 1981.

[18] T J R Hughes. *The Finite Element Method: Linear Static and Dynamic Finite Element Analysis*. Dover Publications, Inc., New York, 2000.

[19] T J R Hughes, M Cohen, and M Haroun. Reduced and selective integration techniques in finite element analysis of plates. *Nuclear Engineering and Design*, 46:203–222, 1978.

[20] T J R Hughes, J A Cottrell, and Y Bazilevs. Isogeometric analysis: CAD, finite elements, NURBS, exact geometry, and mesh refinement. *Computer Methods in Applied Mechanics and Engineering*, 194:4135–4195, 2005.

[21] T J R Hughes and W K Liu. Nonlinear finite element analysis of shells: Part 1. Three-dimensional shells. *Computer Methods in Applied Mechanics and Engineering*, 26:331–362, 1981.

[22] T J R Hughes and W K Liu. Nonlinear finite element analysis of shells: Part 2. Two-dimensional shells. *Computer Methods in Applied Mechanics and Engineering*, 27:167–181, 1981.

[23] T J R Hughes, R L Taylor, and W Kanoknukulchai. Simple and efficient finite element for plate bending. *International Journal for Numerical Methods in Engineering*, 11:1529–1543, 1977.

[24] R L Taylor and S Govindjee. Solution of clamped rectangular plate problems. *Communications in Numerical Methods in Engineering*, 20:757–765, 2004.

[25] S Timoshenko and S Woinowsky-Krieger. *Theory of Plates and Shells*. McGraw-Hill Book Company, Inc., New York, 1959.

# A Appendix A: The One-Dimensional Case

We start by recalling a few notions. For every interval $T := ]c, d[$ and for every integer $r \geq 1$ there exists a polynomial $L_r^T$ of degree $r$ such that

$$\int_T L_r^T(t) p_{r-1}(t) dt = 0 \qquad \forall p_{r-1} \in \mathbb{P}_{r-1}. \tag{106}$$

Such a polynomial is unique up to a multiplicative constant. $L_r^T$ is called the *Legendre polynomial of degree $r$ over $T$*. It can be proved that for each integer $r \geq 1$ there exist exactly $r$ distinct points $g_1^{T,r}, ..., g_r^{T,r}$ (called *Gauss points of degree $r$ over $T$*) internal to $T$ such that

$$L_r^T(g_\gamma^{T,r}) = 0 \qquad \forall \gamma = 1, ..., r. \tag{107}$$

We recall the following result.

**Proposition A.1.** *If $\varphi \in \mathbb{P}_r$ and $\psi \in \mathbb{P}_{r-1}$, then*

$$\Big\{ \int_T (\varphi - \psi) p_{r-1} dt = 0 \; \forall \, p_{r-1} \in \mathbb{P}_{r-1} \Big\} \Leftrightarrow \Big\{ \varphi(g_\gamma^{T,r}) - \psi(g_\gamma^{T,r}) = 0 \; \forall \, \gamma = 1, ..., r \Big\}. \tag{108}$$

In a similar way, for every interval $T$ and for every integer $r \geq 3$ there exists a polynomial $GL_r^T$ of degree $r$ vanishing at the endpoints of $T$ such that

$$\int_T GL_r^T p_{r-3} dt = 0 \; \forall \, p_{r-3} \in \mathbb{P}_{r-3}. \tag{109}$$

Such a polynomial is unique up to a multiplicative constant and is called the *Gauss-Lobatto polynomial of degree $r$ over $T$*. It can be proved that for each integer $r \geq 3$ there exist exactly $r-2$ distinct points $c < \ell_1^{T,r} < \ell_2^{T,r} < ... < \ell_{r-2}^{T,r} < d$ inside $T$ where $GL_r^T$ vanishes. These points are called the *Gauss-Lobatto points of degree $r$ over $T$*. Often, the above notation is extended by setting, for all $r \geq 2$,

$$\ell_0^{T,r} := c, \qquad \ell_{r-1}^{T,r} := d, \tag{110}$$

so that we have

$$c \equiv \ell_0^{T,r} < \ell_1^{T,r} < \ell_2^{T,r} < ... < \ell_{r-2}^{T,r} < \ell_{r-1}^{T,r} \equiv d. \tag{111}$$

Note that for $r = 2$ we have just the two endpoints. Similarly to Proposition A.1 one has now the following result.

**Proposition A.2.** *If $\varphi \in \mathbb{P}_r$ and $\psi \in \mathbb{P}_{r-1}$ coincide at the endpoints of $T$, then*

$$\Big\{ \int_T (\varphi - \psi) p_{r-3} dt = 0 \; \forall \, p_{r-3} \in \mathbb{P}_{r-3} \Big\} \Leftrightarrow \Big\{ \varphi(\ell_\gamma^{T,r}) - \psi(\ell_\gamma^{T,r}) = 0 \; \forall \, \gamma = 1, ..., r-2 \Big\}. \tag{112}$$

Assume now that we are given an interval $T = (a, b)$, and a decomposition $\mathcal{T}_h$ into $K$ subintervals by the nodes

$$a \equiv t_0 < t_1 < ... < t_K \equiv b. \tag{113}$$

We denote by

$$T_k := ]t_{k-1},\, t_k[ \qquad k = 1, ..., K \tag{114}$$

the $k$-th subinterval of the subdivision. As usual, we define

$$h := \max_{k=1,..,K}(t_k - t_{k-1}). \tag{115}$$

In what follows, for the polynomials $L_r^{T_k}$ and $GL_r^{T_k}$ (as well as for the points $g_\gamma^{T_k,r}$ and $\ell_\gamma^{T_k,r}$) on the subinterval $T_k$ we will simply use the index $k$ instead of the index $T_k$. In particular the Gauss points will be denoted by $g_\gamma^{k,r}$, and the Gauss-Lobatto points by $\ell_\gamma^{k,r}$.

For every smooth function $\varphi$ defined on $[a, b]$ and for every integer $r \geq 0$ we define $\Pi_r^G \varphi \in \mathcal{L}_r^0$ as the interpolant of $\varphi$, defined (in $\mathcal{L}_r^0$) by

$$(\Pi_r^G \varphi)(g_\gamma^{k,r+1}) = \varphi(g_\gamma^{k,r+1}), \quad \gamma = 1, .., r+1, \qquad k = 1, ..., K \tag{116}$$

at the Gauss points $g_1^{k,r+1}, ..., g_{r+1}^{k,r+1}$ of $T_k$. Observe that on each subinterval $T_k$ we have:

$$\text{if } \varphi_{|T_k} \in \mathbb{P}_r \text{ then } (\Pi_r^G \varphi)_{|T_k} \equiv \varphi_{|T_k}. \tag{117}$$

This implies that

$$|\varphi - \Pi_r^G \varphi|_{s,T_k} \leq C h^{r+1-s} |\varphi|_{r+1,T_k}, \quad 0 \leq s \leq r. \tag{118}$$

Similarly, for every smooth function $\varphi$ defined on $[a, b]$ and for every integer $r \geq 1$ we define $\Pi_r^{GL} \varphi \in \mathcal{L}_r^1$ as the *continuous* interpolant of $\varphi$, defined (in $\mathcal{L}_r^1$) by

$$(\Pi_r^{GL} \varphi)(\ell_\gamma^{k,r+1}) = \varphi(\ell_\gamma^{k,r+1}), \quad \gamma = 0, .., r, \qquad k = 1, ..., K \tag{119}$$

at the Gauss-Lobatto points $\ell_0^{k,r+1}, ..., \ell_r^{k,r+1}$ of $T_k$. Observe that on each subinterval $T_k$ we have again:

$$\text{if } \varphi_{|T_k} \in \mathbb{P}_r \text{ then } (\Pi_r^{GL} \varphi)_{|T_k} \equiv \varphi_{|T_k}. \tag{120}$$

Hence, as in (118) we have

$$|\varphi - \Pi_r^{GL} \varphi|_{s,T_k} \leq C h^{r+1-s} |\varphi|_{r+1,T_k}, \quad 0 \leq s \leq r. \tag{121}$$

The following result is an immediate consequence of Propositions A.1 and A.2.

**Proposition A.3.** *Let $\varphi \in C^0([a, b])$, let $r$ be an integer $\geq 1$, let $\Pi_r^G \varphi$ be defined as in* (116)*, and, for $r \geq 2$, let $\Pi_r^{GL} \varphi$ be defined as in* (119)*. For every subinterval $T_k$ the following statement holds:*

$$\begin{aligned} &\text{if } \varphi_{|T_k} \in \mathbb{P}_{r+1}(T_k), \text{ then} \\ &\int_{T_k} (\varphi - \Pi_r^G \varphi) p_r \, dt = 0 \quad \text{for all } p_r \in \mathbb{P}_r \text{ and for all } r \geq 1, \end{aligned} \tag{122}$$

$$\int_{T_k} (\varphi - \Pi_r^{GL} \varphi) p_{r-2} \, dt = 0 \quad \text{for all } p_{r-2} \in \mathbb{P}_{r-2} \text{ and for all } r \geq 2. \tag{123}$$

The following proposition is more interesting (see also [2]).

**Proposition A.4.** *Let $\varphi \in C^0([a,b])$, let $r$ be an integer $\geq 1$, and let $\Pi_r^{GL}\varphi$ be defined as in* (119). *For every subinterval $T_k$ the following statement holds:*

$$\text{if } \varphi_{|T_k} \in \mathbb{P}_{r+1}(T_k), \text{ then } \varphi'(g_\gamma^{k,r}) = (\Pi_r^{GL}\varphi)'(g_\gamma^{k,r}), \quad \gamma = 1,..,r, \tag{124}$$

*at the Gauss points $g_1^{k,r},...,g_r^{k,r}$ of $T_k$.*

*Proof.* We set

$$e(t) := \varphi(t) - \Pi_r^{GL}\varphi(t) \qquad \forall t \in [a,b] \tag{125}$$

and observe that, in each interval $T_k$, the definition (119) implies

$$e(t_k) = e(t_{k+1}) = 0. \tag{126}$$

When $\varphi_{|T_k} \in \mathbb{P}_{r+1}$ condition (123) implies

$$\int_{T_k} e(t)p_{r-2}(t)\,dt = 0. \tag{127}$$

Moreover, for $\varphi \in \mathbb{P}_{r+1}$, we obviously have $e' = (\varphi - \Pi_s\varphi)' \in \mathbb{P}_r$. Integrating by parts, using (126), and then using (127), we obtain:

$$\int_{T_k} e'(t)p_{r-1}(t)dt = -\int_{T_k} e(t)(p_{r-1})'(t)\,dt = 0 \quad \forall p_{r-1} \in \mathbb{P}_{r-1}. \tag{128}$$

Hence, from (106) we deduce $e'(t)_{|T_k} = \kappa L_r^k(t)$ for some $\kappa \in \mathbb{R}$, and (124) immediately follows. □

**Remark A.1.** *Observing (rather obviously) that two functions $\psi_1$ and $\psi_2$ coincide at the Gauss points $g_1^{k,r},...,g_r^{k,r}$ for every $k = 1,...,K$ if and only $\Pi_r^G\psi_1 = \Pi_r^G\psi_2$, property* (124) *can also be written as*

$$\Pi_{r-1}^G(\varphi') = \Pi_{r-1}^G(\Pi_r^{GL}\varphi)' \equiv (\Pi_r^{GL}\varphi)'. \tag{129}$$

The following theorem is the one-dimensional analogue of Theorem 5.1 that we want to prove in Appendix B. Before stating it, we introduce, for every integer $m \geq 0$, the so-called *broken norm*

$$\|\phi\|_{m,T,h}^2 := \sum_{k=1}^K \|\phi\|_{m,T_k}^2. \tag{130}$$

**Theorem A.1.** *Let $\varphi$ and $\chi = \varphi'$ be smooth functions, and let $r$ be an integer $\geq 1$. Then there exist two functions $\widehat{\varphi} \in \mathcal{L}_r^1$ and $\widehat{\chi} \in \mathcal{L}_r^1$ such that:*

$$|\varphi - \widehat{\varphi}|_{s,T,h} \leq Ch^{r+1-s}|\varphi|_{r+1,T,h}, \quad 0 \leq s \leq r, \tag{131}$$

$$|\chi - \widehat{\chi}|_{s,T,h} \leq Ch^{r+1-s}|\varphi|_{r+2,T,h}, \quad 0 \leq s \leq r, \tag{132}$$

$$\widehat{\chi}(g_\gamma^{k,r}) = \widehat{\varphi}'(g_\gamma^{k,r}), \quad \gamma = 1,...,r \quad k = 1,...,K. \tag{133}$$

*Proof.* We first take a function $\widetilde{\varphi} \in \mathcal{L}^2_{r+1}$ with the following approximation properties (see Remark A.3 here below):

$$|\varphi - \widetilde{\varphi}|_{s,T,h} \leq C\, h^{r+2-s} |\varphi|_{r+2,T,h}, \quad 0 \leq s \leq r+1. \tag{134}$$

Then, we can define $\widehat{\varphi} := \Pi^{GL}_r \widetilde{\varphi} \in \mathcal{L}^1_r$ as the interpolant of $\widetilde{\varphi}$ defined as in (119), thus verifying

$$|\widetilde{\varphi} - \widehat{\varphi}|_{s,T_k} \leq C\, h^{r+1-s} |\widetilde{\varphi}|_{r+1,T_k}, \quad 0 \leq s \leq r+1, \quad k = 1, .., K. \tag{135}$$

Then by (134), (135), and the triangle inequality we obtain (131). Let us now define $\widehat{\chi} \in \mathcal{L}^1_r$ as

$$\widehat{\chi} := \Pi^{GL}_r \widetilde{\varphi}' \equiv \widetilde{\varphi}', \tag{136}$$

where the last equality holds since $\widetilde{\varphi} \in \mathbb{P}_r$. Hence,

$$|\chi - \widehat{\chi}| = |\varphi' - \widetilde{\varphi}'| \qquad \text{in } [a, b], \tag{137}$$

and the estimate (134) gives the desired (132). Finally, by applying Proposition A.4 to $\widetilde{\varphi}$, we have, at every Gauss point $g^{k,r}_\gamma$,

$$\widehat{\chi}(g^{k,r}_\gamma) \equiv \widetilde{\varphi}'(g^{k,r}_\gamma) = (\Pi^{GL}_r \widetilde{\varphi})'(g^{k,r}_\gamma) \equiv \widehat{\varphi}'(g^{k,r}_\gamma). \tag{138}$$

That is, we have (133). □

**Remark A.2.** *Using the notation of Remark A.1, the equalities in* (138) *can be written as*

$$\Pi^G_{r-1} \widehat{\chi} \equiv \Pi^G_{r-1} \widetilde{\varphi}' = \big(\Pi^{GL}_r \widetilde{\varphi}\big)' \equiv \Pi^G_{r-1} \big(\Pi^{GL}_r \widetilde{\varphi}\big)' \equiv \Pi^G_{r-1}(\widehat{\varphi}'). \tag{139}$$

**Remark A.3.** *For $r \geq 2$, a function $\widetilde{\varphi} \in \mathcal{L}^2_{r+1}$ verifying* (134) *can be easily constructed as a $C^1-$Hermite interpolant of $\varphi$, verifying*

$$\widetilde{\varphi}(t_k) = \varphi(t_k), \quad (\widetilde{\varphi})'(t_k) = \varphi'(t_k) \quad k = 0, \ldots, K, \tag{140}$$

*and, for instance,*

$$\widetilde{\varphi}(g^{k,r-2}_\gamma) = \varphi(g^{k,r-2}_\gamma) \quad k = 1, \ldots, K \quad \gamma = 1, .., r-2 \quad \textit{for } r \geq 3. \tag{141}$$

*This would give, in every $T_k$.*

$$|\varphi - \widetilde{\varphi}|_{s,T_k} \leq C\, h^{r+2-s} |\varphi|_{r+2,T_k}, \quad 0 \leq s \leq r+1, \quad 2 \leq r. \tag{142}$$

*The lowest-order case $r = 1$ needs a different construction, as there is no Hermite-interpolant of degree 2. However, we can define $\widetilde{\varphi}$ as the piecewise quadratic $C^1$ B-spline $s_2(t)$ given by Lemma 3.1 of [3] and verifying*

$$|\varphi - \widetilde{\varphi}|_{s,T_k} = |\varphi - s_2|_{s,T_k} \leq C\, h^{3-s} |\varphi|_{3,\tilde{T}_k,h} \quad 0 \leq s \leq 2, \tag{143}$$

*where $\tilde{T}_k$ is a patch of subintervals made by the union of $T_k$ itself and a fixed number of other subintervals around it. It is clear that both* (142) *and* (143) *easily imply the desired* (134).

# B Appendix B: The Two-Dimensional Case

We recall from (53) the definition of the spaces $\mathcal{L}^{s,\,t}_{[p,\,q]}$:

$$\mathcal{L}^{s,t}_{[p,q]} := \{v \in L^2(\Omega) |\ v(\cdot, y) \in \mathcal{L}^s_p\ \forall y \in ]0, L_2[\,, \text{ and } v(x,\cdot) \in \mathcal{L}^t_q\ \forall x \in ]0, L_1[\,\}. \tag{144}$$

We further recall that $\mathcal{L}^{1,\,1}_{[r,\,r]}$ is the usual finite element space of continuous and locally $\mathbb{Q}_r$ functions. We finally recall that for $r \geq 1$, our finite element spaces are:

$$\boldsymbol{\Theta}^h := \boldsymbol{\Theta}_0 \cap \big(\mathcal{L}^{1,\,0}_{[r,\,r-1]} \times \mathcal{L}^{0,\,1}_{[r-1,\,r]}\big), \tag{145}$$

$$W^h := \mathcal{L}^{1,\,1}_{[r,\,r]}, \tag{146}$$

$$\mathcal{M}^h := \mathcal{L}^{0\,,0}_{[r-1,\,r-1]}. \tag{147}$$

**Proof of Theorem 5.1**

Let $\widetilde{w} \in \mathcal{L}^{2,\,2}_{[r+1,\,r+1]}$ be an approximation of $w$ in the spirit of Remark A.3, such that

$$\sum_{R \in \mathcal{T}_h} |w - \widetilde{w}|_{s,R} \leq C\, h^{t-s} \|w\|_{t,\Omega}, \qquad 0 \leq s \leq t \leq r+2, \quad (\text{with } t > 1). \tag{148}$$

From now on, the generic element $R \in \mathcal{T}_h$ will be individuated by the pair of indices $(i, j)$ for $i = 1, ..., I$ and $j = 1, ..., J$, with obvious meaning of the notation.

We shall often consider the case of different interpolation operators applied to separate coordinates. This will in general be denoted as, say, $(\Pi^G_r, \Pi^{GL}_s)$, meaning that we apply the interpolation operator $\Pi^G_r$ in the $x$ direction and the interpolation operator $\Pi^{GL}_s$ in the $y$ direction. Occasionally, one of the two interpolation operators might be substituted with the identity operator $I$.

We define now $\widehat{w} \in \mathcal{L}^{1,1}_{[r,r]}$ as the *continuous interpolant* of $\widetilde{w}$, defined locally as the interpolant on the tensor-product points (111). That is,

$$\widehat{w} := (\Pi^{GL}_r, \Pi^{GL}_r)\widetilde{w}, \tag{149}$$

or, in more detail,

$$\widehat{w}(\ell^{i,\,r+1}_\alpha, \ell^{j,\,r+1}_\beta) = \widetilde{w}(\ell^{i,\,r+1}_\alpha, \ell^{j,\,r+1}_\beta) \quad \text{ for } \alpha, \beta = 0, ..., r \tag{150}$$

and for $i = 1, ..., I$ and $j = 1, ..., J$. We clearly have

$$|\widetilde{w} - \widehat{w}|_{s,R} \leq C\, h^{r+1-s} |\widetilde{w}|_{r+1,R} \qquad 0 \leq s \leq 1. \tag{151}$$

Using (148), (151), and the triangle inequality, we obtain

$$\sum_{R \in \mathcal{T}_h} \|w - \widehat{w}\|_{1,R} \leq C\, h^r \|w\|_{r+1,\Omega}, \tag{152}$$

that is, (66). We also note that, for every polynomial $q = q_{r-1} \in \mathbb{Q}_{r-1}$, we have by integration by parts

$$\int_R (\widetilde{w}-\widehat{w})_{xy} q \, dx \, dy = \int_{\partial R} (\widetilde{w}-\widehat{w})_x q \, n_y \, dx - \int_{\partial R} (\widetilde{w}-\widehat{w}) q_y \, n_x \, dy + \int_R (\widetilde{w}-\widehat{w}) q_{xy} \, dx \, dy. \quad (153)$$

Integrating by parts the first term in the right-hand side of (153) on each horizontal line (and recalling that $\widetilde{w} - \widehat{w}$ vanishes at the four vertices of $R$), we obtain

$$\int_{\partial R} (\widetilde{w} - \widehat{w})_x q \, n_y \, dx = - \int_{\partial R} (\widetilde{w} - \widehat{w}) q_x \, n_y \, dx. \quad (154)$$

We observe now that $q_x$ has degree $\leq r-2$ in $x$, $q_y$ has degree $\leq r-2$ in $y$, and $q_{xy}$ has degree $\leq r-2$ in both $x$ and $y$. Hence we can use Proposition A.2 to deal with (154) and the second term of (153), and we can use its tensor-product version to deal with the third term of (153). Thus:

$$\begin{aligned} &\int_R (\widetilde{w} - \widehat{w})_{xy} q \, dx \, dy = \\ &- \int_{\partial R} (\widetilde{w} - \widehat{w}) q_x \, n_y \, dx - \int_{\partial R} (\widetilde{w} - \widehat{w}) q_y \, n_x \, dy + \int_R (\widetilde{w} - \widehat{w}) q_{xy} \, dx \, dy \quad (155) \\ &= 0 + 0 + 0 = 0 \qquad \forall q \in \mathbb{Q}_{r-1}, \end{aligned}$$

implying that $\widehat{w}_{xy}$ is the $L^2$ projection of $\widetilde{w}_{xy}$ on $\mathbb{Q}_{r-1}$. Then we have

$$\|\widetilde{w}_{xy} - \widehat{w}_{xy}\|_{0,\Omega} \leq C \, h^r \, \|\widetilde{w}_{xy}\|_{r,\Omega} \leq C \, h^r \, \|w\|_{r+2,\Omega}. \quad (156)$$

The above inequality, together with (148), gives

$$\|w_{xy} - \widehat{w}_{xy}\|_{0,\Omega} \leq C \, h^r \, \|w\|_{r+2,\Omega}. \quad (157)$$

Using the Cauchy-Schwarz inequality and (157) we immediately obtain (67).

In order to define $\widehat{\boldsymbol{\theta}}$, we begin by introducing $\overline{w}_1 \in \mathcal{L}^{2,1}_{[r+1,r]}$, defined by

$$\overline{w}_1(\cdot, \ell^{j,r}_\beta) = \widetilde{w}(\cdot, \ell^{j,r}_\beta) \qquad \beta = 0, .., r, \quad j = 1, ..., J. \quad (158)$$

We may alternatively write

$$\overline{w}_1 = (I, \Pi^{GL}_r)\widetilde{w}. \quad (159)$$

Analogously, we define $\overline{w}_2 \in \mathcal{L}^{1,2}_{[r,r+1]}$ as $\overline{w}_2 := (\Pi^{GL}_r, I)\widetilde{w}$, that is

$$\overline{w}_2(\ell^{i,r}_\alpha, \cdot) = \widetilde{w}(\ell^{i,r}_\alpha, \cdot) \qquad \alpha = 0, .., r, \quad i = 1, ..., I. \quad (160)$$

It is not difficult to see that, for each element $R$, $\overline{w}_1$ coincides with $\widetilde{w}$ whenever $\widetilde{w} \in \mathbb{Q}_r(R)$. It follows that

$$\|\widetilde{w} - \overline{w}_1\|_{s,R} \leq \, C \, h^{r+1-s} \, \|\widetilde{w}\|_{r+1,R}, \qquad 0 \leq s \leq r+1. \quad (161)$$

Similarly, for each element $R$, $\overline{w}_{1,x}$ coincides with $\widetilde{w}_x$ whenever $\widetilde{w}_x \in \mathbb{Q}_r(R)$, implying

$$\|\widetilde{w}_x - \overline{w}_{1,x}\|_{s,R} \leq C\, h^{r+1-s}\, \|\widetilde{w}_x\|_{r+1,R} \leq C\, h^{r+1-s}\, \|\widetilde{w}\|_{r+2,R}, \qquad 0 \leq s \leq r+1. \quad (162)$$

Applying the same arguments to $\overline{w}_2$ one obtains

$$\|\widetilde{w} - \overline{w}_2\|_{s,R} \leq C\, h^{r+1-s}\, \|\widetilde{w}\|_{r+1,R}, \qquad 0 \leq s \leq r+1 \quad (163)$$

and

$$\|\widetilde{w}_y - \overline{w}_{2,y}\|_{s,R} \leq C\, h^{r+1-s}\, \|\widetilde{w}_y\|_{r+1,R} \leq C\, h^{r+1-s}\, \|\widetilde{w}\|_{r+2,R}, \qquad 0 \leq s \leq r+1. \quad (164)$$

It is *very important* to note that $\widehat{w}$, defined as the interpolant of $\widetilde{w}$ in (150), can actually be considered as the interpolant of either $\overline{w}_1$ or $\overline{w}_2$ as well, i.e.,

$$\widehat{w} := \widetilde{w}^I \equiv \overline{w}_1^I \equiv \overline{w}_2^I, \quad (165)$$

as the three functions $\widetilde{w}$, $\overline{w}_1$, and $\overline{w}_2$ coincide at the tensor product of the Gauss-Lobatto points in each element. Using the alternative notation of Remark A.1, we can write

$$\widehat{w} = (\Pi_r^{GL}, \Pi_r^{GL})\widetilde{w} = (\Pi_r^{GL}, \Pi_r^{GL})\Big((I, \Pi_r^{GL})\widetilde{w}\Big) = (\Pi_r^{GL}, \Pi_r^{GL})\Big((\Pi_r^{GL}, I)\widetilde{w}\Big). \quad (166)$$

We also point out that both

$$(\overline{w}_1)_x \in \mathcal{L}^{1,1}_{[r,r]} \quad \text{and} \quad (\overline{w}_2)_y \in \mathcal{L}^{1,1}_{[r,r]}. \quad (167)$$

We can finally define $\widehat{\boldsymbol{\theta}} \in \mathcal{L}^{1,0}_{[r,r-1]} \times \mathcal{L}^{0,1}_{[r-1,r]}$ as:

$$\begin{aligned} &\widehat{\theta}_1(\cdot,\, g_\beta^{j,r}) = (\overline{w}_1)_x(\cdot,\, g_\beta^{j,r}), \quad \beta = 1,..,r, \\ &\widehat{\theta}_2(g_\alpha^{i,r},\, \cdot) = (\overline{w}_2)_y(g_\alpha^{i,r},\, \cdot), \quad \alpha = 1,..,r. \end{aligned} \quad (168)$$

Alternatively, we may write $\widehat{\theta}_1 := (I, \Pi_r^G)(\overline{w}_1)_x$ and $\widehat{\theta}_2 := (\Pi_r^G, I)(\overline{w}_2)_y$.

It is not difficult to check that, in each element $R$, both mappings $(\overline{w}_1)_x \to \widehat{\theta}_1$ and $(\overline{w}_2)_y \to \widehat{\theta}_2$ coincide with the identity mapping whenever $(\overline{w}_1)_x$ (respectively, $(\overline{w}_2)_y$) is in $\mathbb{Q}_{r-1}(R)$, implying that

$$\|\overline{w}_{1,x} - \widehat{\theta}_1\|_{s,\,R} + \|\overline{w}_{2,y} - \widehat{\theta}_2\|_{s,\,R} \leq C\, h^{r-s}\, (\|\overline{w}_{1,x}\|_{r,R} + \|\overline{w}_{2,y}\|_{r,R}). \quad (169)$$

At the same time, in each element $R$, $\widehat{\theta}_{1,x}$ coincides with $\overline{w}_{1,xx}$ whenever $\overline{w}_{1,xx} \in \mathbb{Q}_{r-1}(R)$, and $\widehat{\theta}_{2,y}$ coincides with $\overline{w}_{2,yy}$ whenever $\overline{w}_{2,yy} \in \mathbb{Q}_{r-1}(R)$. Hence,

$$\|\overline{w}_{1,xx} - \widehat{\theta}_{1,x}\|_{s,\,R} + \|\overline{w}_{2,yy} - \widehat{\theta}_{2,y}\|_{s,\,R} \leq C\, h^{r-s}\, (\|\overline{w}_{1,xx}\|_{r,R} + \|\overline{w}_{2,yy}\|_{r,R}). \quad (170)$$

Combining (169) and (170) with (161)-(164) and recalling the norm defined in (10), we obtain for each element $R$

$$\|\widehat{\boldsymbol{\theta}} - \nabla\widetilde{w}\|_{(H_x,H_y),\,R} \leq C\, h^r \|\widetilde{w}\|_{r+2,\,R}. \quad (171)$$

To complete the proof, we have to deal with the crucial requirement (68) which in our case can be written as $(\Pi^G_{r-1}, \Pi^G_{r-1})\widehat{\boldsymbol{\theta}} = (\Pi^G_{r-1}, \Pi^G_{r-1})\nabla\widehat{w}$ or, alternatively,

$$\widehat{\boldsymbol{\theta}}(g^{i,r}_\alpha, g^{j,r}_\beta) = \nabla\widehat{w}(g^{i,r}_\alpha, g^{j,r}_\beta) \tag{172}$$

for $\alpha, \beta = 1, .., r$, $i = 1, .., I$, and $j = 1, .., J$. Let us consider the first component of the above expression. For each each horizontal edge $y = \ell^{j,r+1}_\beta$ $(\beta = 0, .., r)$, we have that $\overline{w}_1$ and $\widetilde{w}$ coincide. Thus, as already pointed out in (165), $\widehat{w} \equiv \Pi^{GL}_r \overline{w}_1$. Hence we can apply Proposition A.4 to obtain

$$\widehat{w}_x(g^{i,r}_\alpha, \ell^{j,r+1}_\beta) = (\overline{w}_1)_x(g^{i,r}_\alpha, \ell^{j,r+1}_\beta) \quad \alpha = 1, .., r, \quad \beta = 0, .., r. \tag{173}$$

Considering the vertical lines $x = g^{i,r}_\alpha$, we now have that both $\widehat{w}_x$ and $(\overline{w}_1)_x$ are polynomials of degree $r$ in $y$. Hence, as they coincide at $y = \ell^{j,r+1}_\beta$ for $\beta = 0, .., r$, they must coincide on the whole line and, in particular, at the Gauss points $g^{j,r}_\beta$ (for $\beta = 1, .., r$). That is,

$$\widehat{w}_x(g^{i,r}_\alpha, g^{j,r}_\beta) = (\overline{w}_1)_x(g^{i,r}_\alpha, g^{j,r}_\beta) \quad \alpha = 1, .., r, \ \beta = 1, .., r. \tag{174}$$

On the other hand, for each horizontal line $y = g^{j,r}_\beta$, we have that $\widehat{\theta}_1$ and $(\overline{w}_1)_x$ coincide on the whole line (and consequently at the Gauss points) by invoking the first equation of (168). Hence, (174) implies the first component of (172). We obtain the second component of (172) using a similar argument, completing the proof. □